

Article

Compression Behavior of Sheets Metals of Pure Titanium 2 and Ti6Al4V Alloy under High Temperature: Evaluation of the Tension–Compression Asymmetry

Jorge Ayllón^{1,2}, Valentín Miguel^{1,2,*}, Alberto Martínez-Martínez¹, Juana Coello^{1,2}, Jesús Andrés Naranjo^{1,2} and Francisco García-Sevilla^{1,2}

¹ Regional Development Institute, Material Science and Engineering, University of Castilla-La Mancha, 02006 Albacete, Spain; jorge.ayllon@uclm.es (J.A.); alberto.martinez@uclm.es (A.M.-M.); juana.coello@uclm.es (J.C.); jesus.naranjo@uclm.es (J.A.N.); francisco.garcia@uclm.es (F.G.-S.)
² Industrial Engineering School of Albacete, University of Castilla-La Mancha, 02006 Albacete, Spain
* Correspondence: valentin.miguel@uclm.es; Tel.: +34-967-599-200

Abstract: Determining the intrinsic indices of sheet metals under compression states at high temperatures is vital to accurately predict the behavior of the material in warm/hot forming processes. Nevertheless, the literature contains little previous experimental data in this regard due to the difficulty of carrying out specific test methodologies in sheet metals. The authors of the present manuscript previously developed an approach to evaluate the in-plane compression behavior under a wide range of test conditions, which was applied here to characterize pure titanium and Ti6Al4V alloy until 750 °C. This procedure allowed us to quantify the asymmetric and anisotropic tension–compression (T-C) response of the materials involved and their evolution with temperature and strain rate. The asymmetry detected at room temperature showed a higher compression response in all cases, mostly reaching differences of around 10%. For the lowest strain rate studied, the typical assumed symmetric T-C behavior was observed from 300 and 450 °C onwards, for the rolling and transverse direction, respectively. In addition, stepped compression tests led us to deduce the anisotropy indices, which were different from those found under tension, in contrast to the r-values applied by most authors. Using the experimental results, a factor related to the asymmetry found was proposed to formulate an extended constitutive model. The asymmetry and anisotropy data supplied for compression under warm/hot conditions are the main novelty of this research.

Keywords: sheet metal compression; tension-compression asymmetry; high temperature; compression anisotropy; titanium alloys



Citation: Ayllón, J.; Miguel, V.; Martínez-Martínez, A.; Coello, J.; Naranjo, J.A.; García-Sevilla, F. Compression Behavior of Sheets Metals of Pure Titanium 2 and Ti6Al4V Alloy under High Temperature: Evaluation of the Tension–Compression Asymmetry. *Metals* **2021**, *11*, 168. <https://doi.org/10.3390/met11010168>

Received: 27 December 2020
Accepted: 15 January 2021
Published: 18 January 2021

Publisher's Note: MDPI stays neutral with regard to jurisdictional claims in published maps and institutional affiliations.



Copyright: © 2021 by the authors. Licensee MDPI, Basel, Switzerland. This article is an open access article distributed under the terms and conditions of the Creative Commons Attribution (CC BY) license (<https://creativecommons.org/licenses/by/4.0/>).

1. Introduction

Titanium alloy sheets are used in a large number of applications with high technological value within the aeronautical, biomedical, and energy sectors. This is due to their good resistance–density ratio, corrosion resistance, or biocompatibility [1–3]. However, due to their low Young's modulus and high yield stress, forming these materials presents a high springback, which makes it difficult to obtain products with good dimensional accuracy. Moreover, most titanium alloys exhibit limited conformability at room temperature. All these factors mean that parts need to be formed in hot working conditions [4].

The deformation mechanisms of titanium alloys at room temperature and in general, of materials based on hcp-structures have been widely reported in the literature. This crystallographic structure is characterized by a highly anisotropic behavior due to its limited ability to accommodate deformations by sliding mechanisms. In this way, twinning takes place as an additional mechanism to achieve free deformation, with the main twinning systems being different for tensile and compression states [5]. The twinning polarity together with a strong texture, which is consequence of prior thermo-mechanical

processes, significantly influence the strain hardening due to crystallographic reorientation [6], the Hall–Petch effect, and the Basinski hardening mechanism [7]. Some authors suggest that this phenomenon is one of the reasons for the tension–compression asymmetry behavior observed [6,8]. However, this fact is controversial due to the contribution that directional sliding mechanisms, and their interactions with the twinning, have on the deformation [9]. For Ti6Al4V, the addition of Al causes the twinning not to be a major deformation mechanism, so it is difficult to fully attribute to it the asymmetry phenomenon of this material [10–12].

Twinning affects the deformation of titanium alloys, presenting several strain stages according to the dominant deformation mechanisms. Nemat-Nasser et al. [13] found three hardening stages for extruded pure titanium in compression tests. They correlated a high temperature and/or a low strain rate with the non-existence of twinning mechanism in the strain. The first stage is dominated by a prismatic and basal slip and is defined at the earlier strain; the second stage responds to a significant twinning phenomenon and, finally when this effect stabilizes, the third stage begins [14]. Therefore, a minimum quantity of previous deformation is necessary for twinning nucleation [15,16]. At temperatures above 500 °C, Zeng et al. [17] observed that the three-stage hardening of pure titanium disappears, and the pyramidal slip $\langle a + c \rangle$ replaces twinning as the main compression deformation mechanism. This is consistent with the importance of $\langle a + c \rangle$ slip in the titanium polycrystals deformation at high temperature detected by Paton and Backofen [16]. However, under tensile conditions, Roth et al. [9] described that the three-stage strain hardening of titanium may be due to anisotropic nature of dislocation glide and not to twinning. Furthermore, Nixon et al. [18] observed that this asymmetry is highly dependent on the sheet metal direction. The difference in the predominant twinning modes, $\{10\bar{1}2\}$ for rolling direction (RD) and $\{11\bar{2}2\}$ for transverse direction (TD), and a greater concentration of poorly oriented grains in one direction, which implies a greater hardening by reorientation, are the causes of this variation [19]. In addition, twinning is much more significant for the transverse direction, which causes the values of tension and compression obtained to be greater than in the case of rolling direction [5,9,18]. No previous works have focused on evaluating the asymmetry phenomenon at temperatures above room temperature, especially for titanium sheet metal. Only for magnesium alloys a reference has been found [20], and even in this study, the maximum temperature considered was 300 °C, which is technically affordable without great complexity.

In addition to the asymmetric tension–compression (T-C) character of the titanium alloys, it is important to identify the anisotropy (r), especially for sheet metals whose indices are strongly determined by the previous rolling procedure. This anisotropic behavior is due to the limited capacity for accommodating the deformations and because, as mentioned, the deformation mechanisms are different in tension and compression. Thus, r -values in tension and compression need not necessarily be equal [21], as some authors assume in their research [22]. Despite the expected importance of this aspect, no models have been developed that include specific r -values for compression stresses. Moreover, very few studies have obtained this parameter. For example, Zhou et al. [23] determined the compression r -values for AZ31B magnesium sheet alloy and found that the values were very different than the tensile ones, with these being higher.

The anisotropy and asymmetry existing in titanium alloys demand complex behavior models to obtain accurate results in the forming analysis [24,25]. The definition of these models would require experimental data correctly obtained for the different stress states. Sheet metal compression is probably one of the least studied stress states. One of the reasons for the lack of compressive experiments with sheet metals could be the complexity of the methodology to be used, especially if temperature is involved. Two main methodological lines can be distinguished. The first one was suggested by Boger et al. [26], who designed a test system based on two lateral anti-buckling plates using a specific shape for the sample. The second line was originally proposed by Kuwabara et al. [27], which used comb-shaped

clamps for achieving higher strains. Both guidelines have been followed by many authors for compression tests at room temperature.

Nevertheless, research on sheet metal compression at warm/high temperatures is insufficient. Piao et al. [28] modified Boger's design, adding a heating system inside the lateral anti-buckling plates. They were able to evaluate the T-C behavior of AZ31B magnesium alloy, TWIP (Twinning-Induced Plasticity), and DP (Dual-Phase)-steels up to 250 °C, determining the Bauschinger effect on these materials. Lee et al. [29] developed a similar solution, but considering Kuwabara's design, and validated the influence of T-C asymmetry on the springback phenomenon at a warm temperature (200 °C). Liu et al. [20] planned another alternative configuration consisting of employing an insulated cabinet to heat the sample during the compression test, reaching a temperature of 300 °C. They demonstrated that the existent T-C asymmetry at room temperature for the AZ31B magnesium alloy tended to disappear at higher temperatures. Running the test in a furnace makes it easier to control the temperature and simplifies the procedure. All these features, and the need to widen the field of temperatures involved in compression tests, led the authors of the present work to establish a relatively simple methodology for testing sheet metals at higher temperatures [30]. This procedure was validated at room temperature through the analysis of six different alloys. To this end, an inverse modeling approach was used that avoided the measurement of the material strains during the test, which is especially difficult at high temperature.

The present work consists of the application of the above-mentioned methodology to obtain, at several temperatures, the asymmetric tension–compression behavior of the most commonly used titanium alloys, commercial pure titanium grade 2 and Ti6Al4V. The influence of the strain rate on the results was also considered. In addition, the Lankford or anisotropy index was determined. The analysis and evaluation of both aspects, asymmetry and anisotropy, under high temperature compressive conditions, is a scientific and technological novelty in this field. Moreover, the results obtained under tension conditions are valuable, as they broaden and reinforce the existing knowledge in the area.

2. Materials and Methods

2.1. Materials

The tensile and compressive behavior of two titanium alloys was studied: commercial pure titanium grade 2 (Ticp2) (ASTM B265) and Ti6Al4V alloy (AMS 4911 N). Ticp2 was supplied as a cold rolled and annealed sheet and Ti6Al4V was supplied as a mill-annealed sheet. Both sheets were 0.8 mm thick. The chemical composition and the as-received micro-structures of both materials are shown in Table 1 and Figure 1. In Figure 1a, the microstructure of Ticp2 can be seen and consists of an α -phase with an average grain size of 40.7 μm . Figure 1b represents the biphasic $\alpha + \beta$ structure corresponding to the Ti6Al4V alloy. In this material, the α grains, with a mean size of 7.2 μm are embedded in intergranular fine β -phase. Some grade of grain deformation in the rolling plane can be appreciated properly for Ti6Al4V.

Table 1. Chemical composition of the analyzed titanium alloys (wt.%).

| Material | Ti | V | Al | Fe | C | O | N | Y | H | O + H |
|----------|-----------|-----------|-----------|-----------|-------------|-----------|-------------|---------|-------|-----------|
| Ticp2 | Remainder | - | - | 0.09–0.10 | 0.01 | 0.14–0.15 | <0.01 | - | 0.002 | - |
| Ti6Al4V | Remainder | 4.01–3.97 | 6.19–6.16 | 0.18–0.16 | 0.017–0.014 | 0.20–0.19 | 0.008–0.007 | <0.0004 | - | 0.21–0.20 |

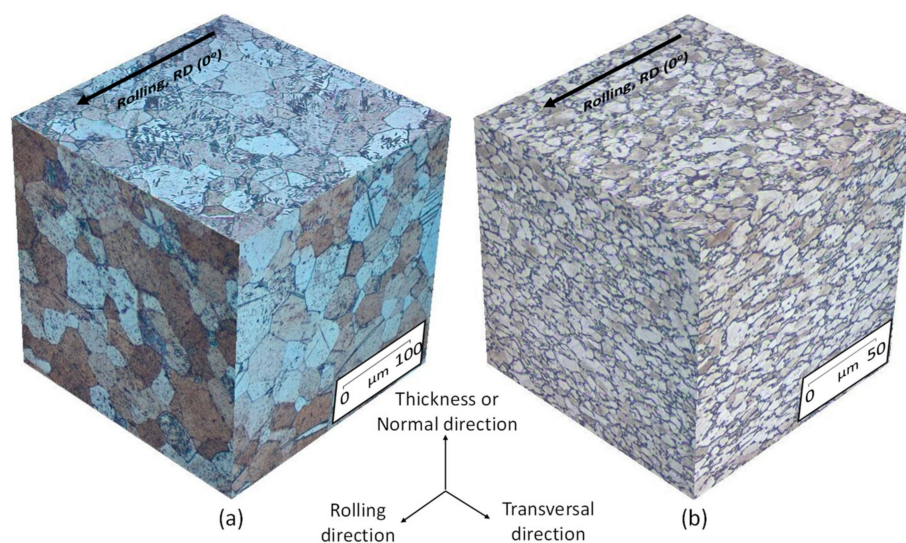


Figure 1. As-received micro-structure considering the different directions respect to rolling one. (a) α -phase of TiCp2 (200 \times); (b) $\alpha + \beta$ phases of Ti6Al4V (400 \times).

2.2. Tensile Tests

Isothermal tensile tests were carried out using a universal testing machine, Servosis ME 401/10 \pm 100 kN (SERVOSIS Inc., Madrid, Spain), equipped with a furnace that permits temperatures of up to 1000 $^{\circ}$ C to be reached. These tests were conducted according to the procedure established in the EN ISO 6892-2 standard [31], using the test samples detailed in Figure 2a. Temperatures of 25, 300, 450, 600, and 750 $^{\circ}$ C and strain rates of 0.002, 0.02, and 0.2 s^{-1} were selected as experimental parameters. All the tests were performed for the main directions of the sheet, i.e., rolling direction (0 $^{\circ}$ or RD) and transverse direction (90 $^{\circ}$ or TD). To ensure a homogeneous temperature of the material, the samples were kept 10 min in the furnace before the test. Although no protection was applied to the samples, no severe oxidation indicating deterioration of the mechanical parameters was observed.

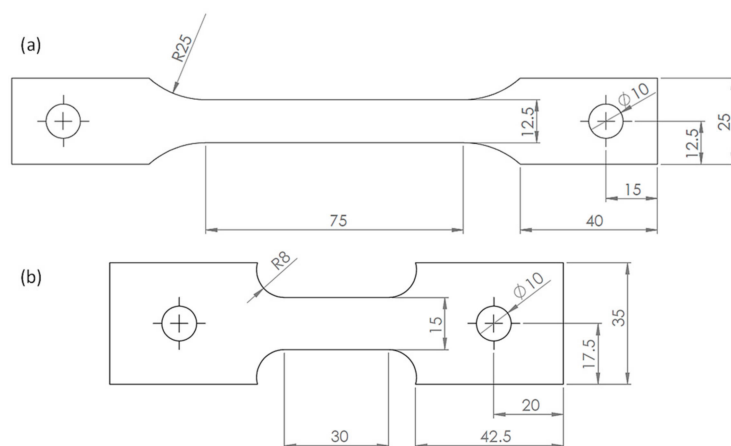


Figure 2. Test specimens used (dimensions in mm). (a) Tensile sample; (b) compression sample.

The engineering curves obtained were turned into true stress–strain curves up to the onset of the necking or the Ultimate Tensile Strength point (UTS), employing the standard procedure [30]. The homogeneous plastic strain zone was adjusted to a Swift function and extrapolated beyond the necking point until failure, as shown in Equation (1), where n is the strain hardening index, K is the strength coefficient and ε_0 is the elastic strain.

$$\sigma = K \left(\varepsilon_0 + \varepsilon_{pl} \right)^n \quad (1)$$

In addition to the tensile tests, anisotropy was determined according to the EN ISO 10113 standard [32]. The specimens were deformed at a strain rate of 0.002 s^{-1} for all analyzed temperatures. To determine the anisotropy index during the uniform deformation range, interrupted tests were performed up to different strain values until that of the necking point was reached.

2.3. Compression Tests

The compression tests were carried out under the same conditions as the previous tensile tests to observe the possible T-C asymmetries. The sheet compression sample shown in Figure 2b was used. This test specimen permits work to be performed in a quasi-uniaxial compression state, avoiding buckling until high deformation values [30].

In view of the specimen dimensions, test speeds of 4, 40, and 400 mm/min were chosen, which represent approximate constant strain rates of 0.002, 0.02, and 0.2 s^{-1} , which are similar to those defined in the tensile tests. For a strain rate of 0.002 s^{-1} , additional tests were performed up to different plastic strain levels. This allowed the repeatability of the procedure to be quantified, as well as allowing the anisotropy values for compressive strains (r_0 and r_{90}) to be obtained.

Due to the non-uniform deformation observed in the compression samples, it was not possible to indirectly evaluate the thickness strains, as proposed by EN ISO 10113 standard [32]. This led to the necessity of determining this strain by direct measurement, using a micrometer with a standard uncertainty $\leq 0.01 \text{ mm}$.

To carry out the compression tests, comb-type dies, previously designed by the authors (Figure 3a,b), were used [30]. The dies were located in the furnace during the tests, which allowed temperatures of up to $800 \text{ }^\circ\text{C}$ to be reached (Figure 3c). This system simplifies the method used by other authors [28,29], as the furnace isolation makes any additional temperature control system unnecessary. Nevertheless, a setup operation was carried out, using external thermocouples, to check the temperature homogeneity in the chamber. Due to the mass involved, it was necessary to keep the assembly inside the furnace for 15–20 min in order for the sample to achieve a uniform temperature.

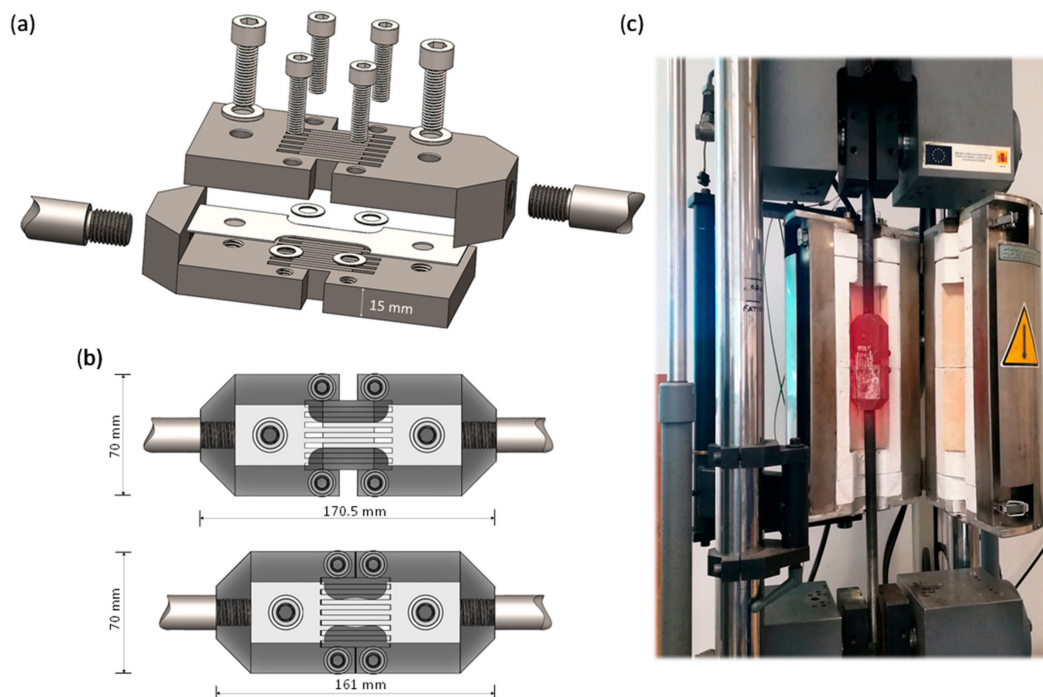


Figure 3. (a) Schematic of the assembly for compression tests [30]. (b) Initial and final (maximum achievable compression) stages of operation. (c) Compression device after a test at $750 \text{ }^\circ\text{C}$.

The tightening torque of the main screws was sufficient to guarantee the joint of the dies under the temperature of the tests. Moreover, the goal of the lateral screws was to avoid elastic gaps in the test area (Figure 3a). In any event, the behavior of the system may be considered to have been similar in all cases, at least when temperature of the test was the same.

2.4. High-Temperature Lubricant Selection

The proposed compression tests require the reduction of the friction forces in the system, with it being necessary to use lubricants. However, the choice of lubricants is limited due to the need to work in a high-temperature range. Based on the experience of the use of solid lubricants in hot forming operations, and given their advantages, MoS₂ (molybdenum disulfide) and h-BN (hexagonal boron nitride) were selected [33].

In order to characterize the tribological behavior of these lubricants and to establish appropriate ranges of application, pin-on-disk tests were performed at different temperatures and velocities for the steel–titanium friction pair. Lubricants were applied in the same way in both the friction tests and the compression tests. To this end, the particles were dispersed in alcohol first, and the surfaces were primed. In this way, the evaporation of the solvent resulted in a uniform layer of MoS₂ or h-BN adhered on the surface. Friction tests without using lubricant were also carried out to quantify the improvement generated by the use of lubricants. The temperature values selected for these tests were 25, 300, 450, and 600 °C, and the velocity values were 6, 47, 94, 471, and 848 mm/min. For all tests, a load of 50 N was established, which resulted in a constant average pressure of 20–30 MPa. With this selection of variables, the conditions of the compression tests were reproduced.

The friction coefficients obtained from these tests are shown in Figure 4. In view of the limited influence of velocity on the friction coefficient, this variable was removed to simplify the analysis. Therefore, the friction coefficient for each temperature was taken as the average value, regardless of the velocity considered.

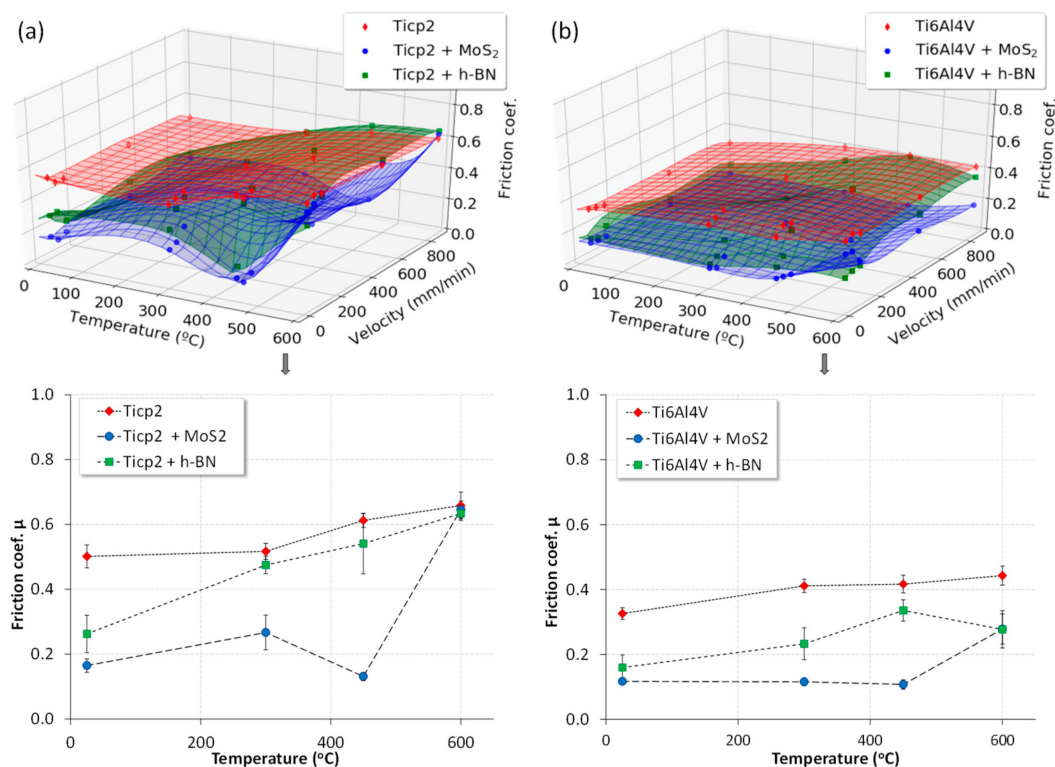


Figure 4. Friction coefficients obtained: (a) Ticp2; (b) Ti6Al4V.

As can be seen, MoS₂ provides the best friction conditions up to 450 °C. Friction coefficients of around 0.2 in the case of Ticp2 and 0.1 in the case of Ti6Al4V were obtained, which means the friction force is reduced by about 65% and 70%, respectively. However, there is a marked change at 600 °C, which must be attributed to the decomposition and oxidation of MoS₂. This was confirmed by the Thermogravimetric and Differential Thermal Analysis, TG-DTA EXSTAR 6000 (Seiko Instruments Inc., Chiba, Japan), (Figure 5), which showed an exothermic degradation of MoS₂ at 450–500 °C. In the case of h-BN, the obtained values were not so good and presented higher dispersion, although they still represent an improvement of 5–30% in the case of Ticp2 and 20–50% for Ti6Al4V, depending on the temperature. However, as can be seen in Figure 5, this lubricant is an inert compound over the whole temperature range. This implies stable behavior, regardless of the working time at high temperature, which is not the case with MoS₂.

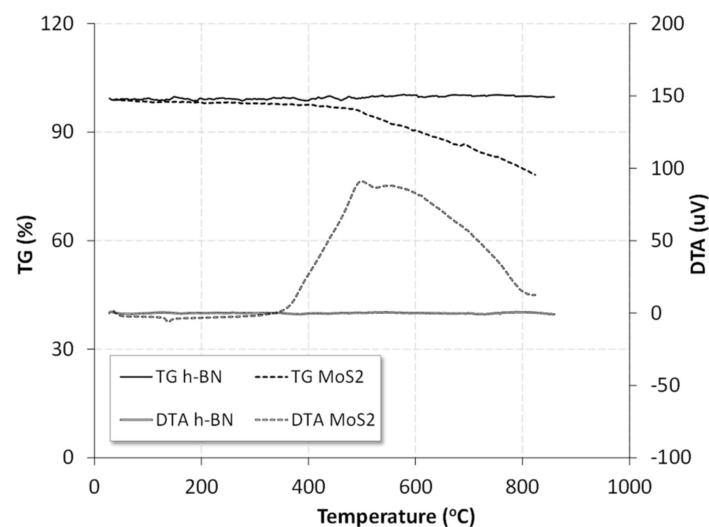


Figure 5. Thermogravimetric and Differential Thermal Analysis (TG-DTA) analysis of the employed lubricants: MoS₂ and h-BN.

In view of the results obtained, it was concluded that MoS₂ is the most suitable lubricant for application up to 450 °C. The stability of h-BN favors its use at higher temperatures. However, both lubricants were used at 600 °C to overlap their ranges of use.

2.5. Evaluation of the Friction Component in Compression Tests

Due to the characteristics of the compression system, it was necessary to control and evaluate the friction appearing during the test in the die–specimen–die contact, as the result of the specimen shortening in compression. In addition, some die–die sliding also occurs, which causes friction that must also be evaluated. Although some authors neglect the friction influence on the test [27], this is not possible at high temperatures, and it is important to take this phenomenon into account.

To determine the average friction force, specific tests were carried out, consisting of applying tensile forces to the compression die–specimen–die assembly at the same conditions as those in compression tests. From the results herein obtained, the typical tensile behavior of the material was subtracted, and the average friction force was determined, as shown in Figure 6a [30].

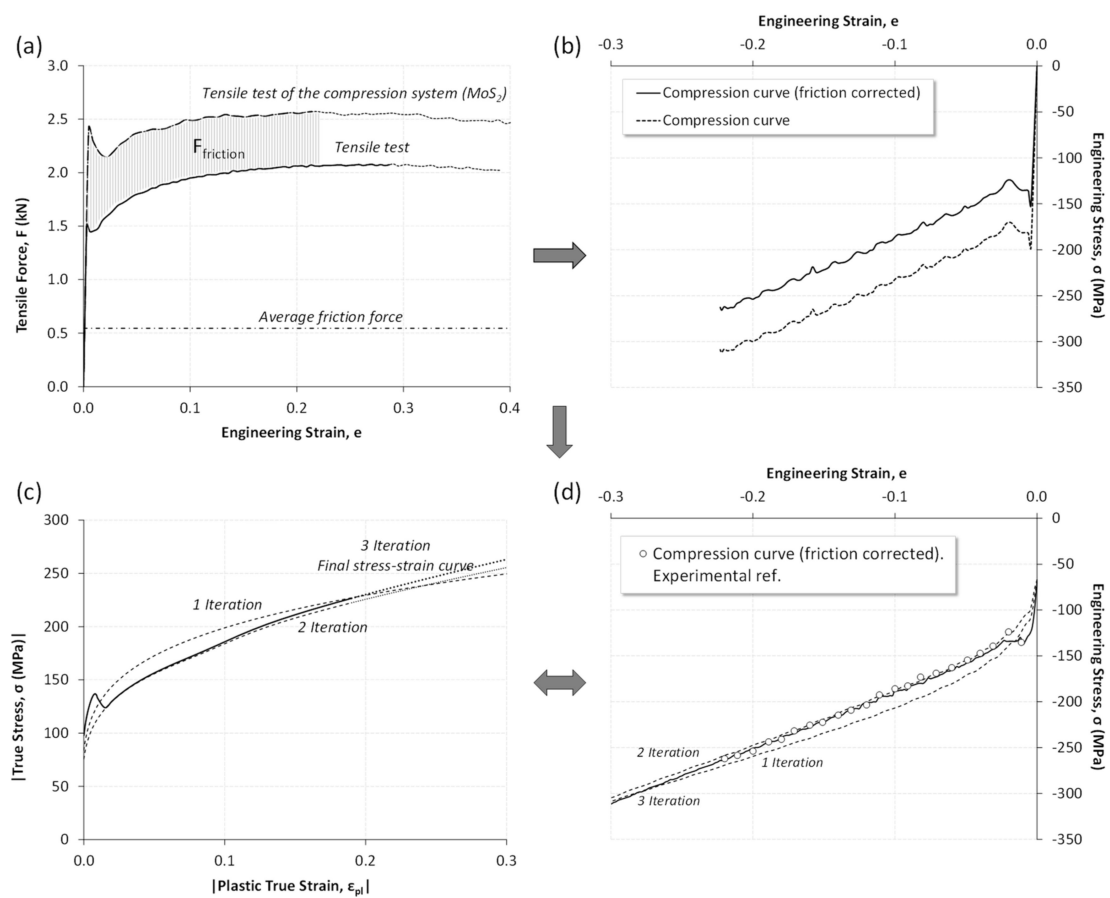


Figure 6. Processing procedure of the compression stress–strain curve of Ticp2 at 300 °C and 0.002 s^{−1}. (a) Determination of the friction force by means of specific tensile tests; (b) frictional force correction in the compression curve; (c) iterative steps corresponding to the inverse method; (d) engineering curve obtained after each iteration of the inverse method.

2.6. Determining the Compression True Stress–Strain Behavior

The compression engineering stress–strain curves were determined by subtracting the average friction force from the compression tests results (Figure 6b). Finally, the true compressive curves were obtained by using an inverse modeling method, since the non-uniform deformation produced in the samples prevents the application of the traditional equations. This methodology consists of an FEM iterative approach (Figure 7), with which the true stress–strain curve must be modified until the simulation-predicted engineering curve is equal to the experimental one [30].

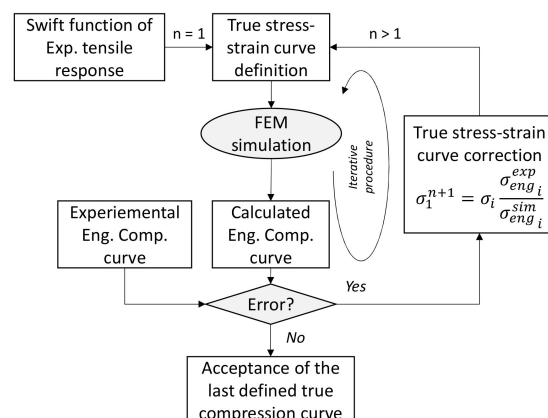


Figure 7. Flow chart of the inverse method used for the determination of the compression curve.

The simulations were run using the explicit software Hypermesh + Radioss (Altair Engineering Inc., Troy, MI, USA). The model of the specimen consisted of 2D quad QEPH type elements of 1 mm in size, that is, a standard Radioss element improved and under-integrated with physical hourglass stabilization. As demonstrated [30], the simulations performed according to the Von Mises yield criterion were valid and simplified the procedure.

Initially, the material was modeled according to the Swift function obtained by the previous tensile tests for each temperature, as shown in Equation (1). In each iteration, the reference experimental engineering stress–strain curve was compared with those predicted by the FEM simulation (Figure 6d). For an elongation point, the experimental, $\sigma_{eng_i}^{exp}$, and simulated, $\sigma_{eng_i}^{sim}$, engineering stresses and the average simulated plastic strain, $\bar{\epsilon}_{pl_i}^{sim}$, in the cross-central section were obtained. For every plastic strain value, $\bar{\epsilon}_{pl_i}^{sim}$, the new compressive true stress value was calculated using Equation (2). By applying this procedure in all plastic strain points, i , the true curve was corrected at each iteration, n , as shown in Figure 6c.

$$\sigma_i^{n+1} = \sigma_i^n \cdot \frac{\sigma_{eng_i}^{exp}}{\sigma_{eng_i}^{sim}} \quad (2)$$

Applying this procedure, in no case were more than three iterations needed to obtain good agreement between the experimental reference curve and that predicted by FEM simulation.

3. Results and Discussion

3.1. Asymmetric Tension–Compression Behaviour Depending on Temperature

According to the previous considerations, the compression behavior of Ticp2 and Ti6Al4V was evaluated at a range of temperatures of 25–750 °C and a strain rate value of 0.002 s^{−1}, as shown in Figures 8 and 9, respectively. These figures depict, for the corresponding material, the experimental true tensile and compressive behavior. The compressive results are expressed by an average curve and a deviation band. Regarding the tensile curves, two different shapes from the necking point on can be pointed out: an extrapolation of the curve by applying the Swift function, and the other by considering the traditional engineering true transformation (Figure 8a). As is widely known, this last conversion is typically meaningless, as it is only valid until the necking point. Nevertheless, this part of the graphic results is relevant if the necking point cannot easily be located, as sometimes occurs at a high temperature [34,35].

Related to the compression behavior, the mean curve was obtained from the different tests carried out under the same conditions (between five and seven tests). The band represents the standard deviation involved for each point of the mean curve. Logically, the bandwidth is an index of the repeatability or the typical uncertainty of the methodology used, and it is quantified in Figure 10. As can be seen, the absolute average deviation is considerably similar for all temperatures, which means that the uncertainty of the experimental methodology is independent of that variable. Nevertheless, the results are more precise for low temperatures if the deviation is considered in relative terms of the total stress involved in each case.

According to the maximum temperature of use of MoS₂, the tests at 600 °C were conducted with both lubricants (MoS₂ and h-BN) (Figure 8g,h and Figure 9g,h). The corrected results are similar for both cases as the effect of friction is properly removed.

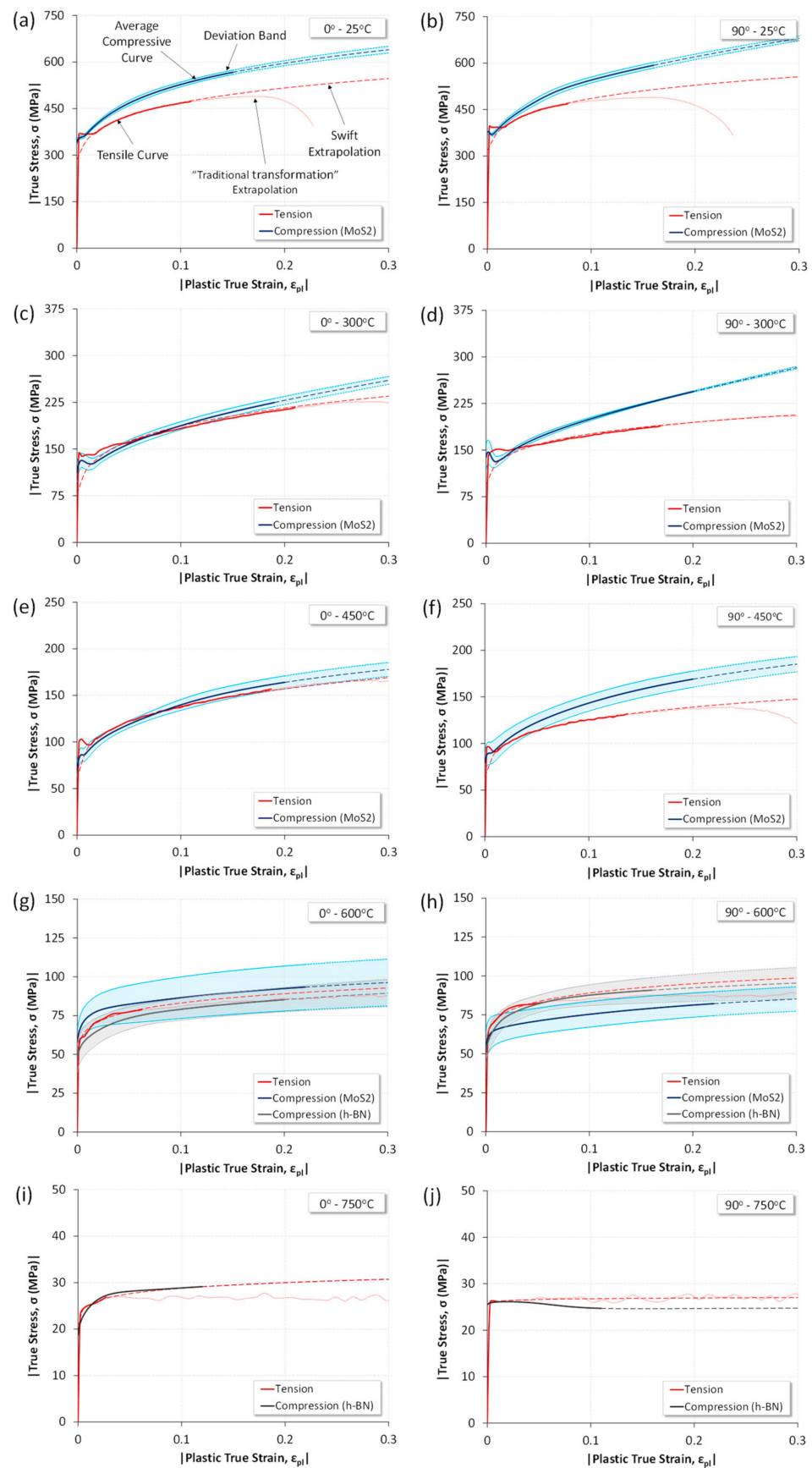


Figure 8. Tension and compression mechanical curves of T1cp2 at 0.002 s^{-1} and temperatures of 25, 300, 450, 600, and 750 °C. (a,c,e,g,i) Mechanical behavior in rolling direction (0°); (b,d,f,h,j) Mechanical behavior in transverse direction (90°).

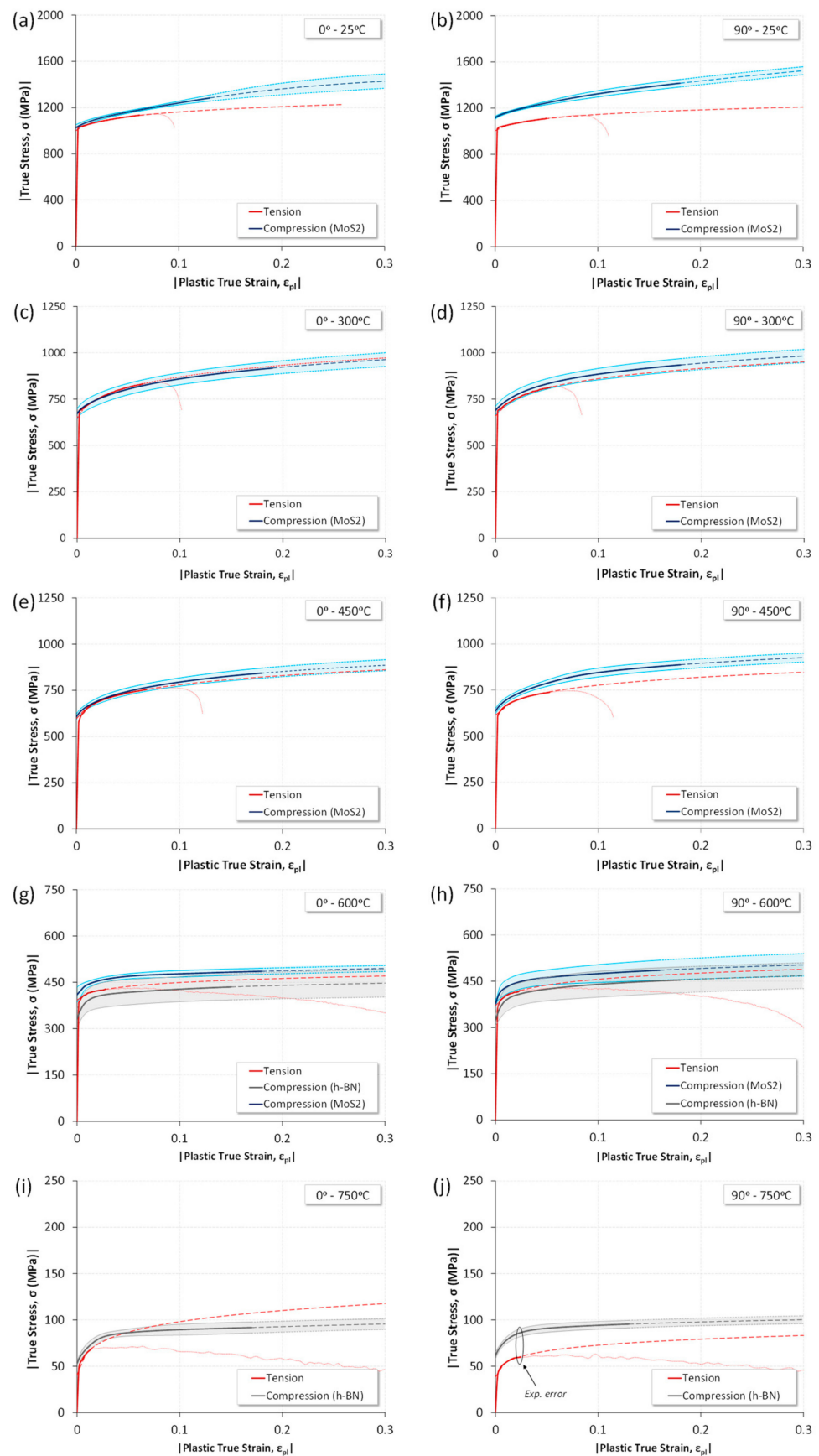


Figure 9. Tension and compression behavior of Ti6Al4V at 0.002 s^{-1} and temperatures of 25, 300, 450, 600, and 750 °C. (a,c,e,g,i) Mechanical behavior in rolling direction (0°); (b,d,f,h,j) Mechanical behavior in transverse direction (90°).

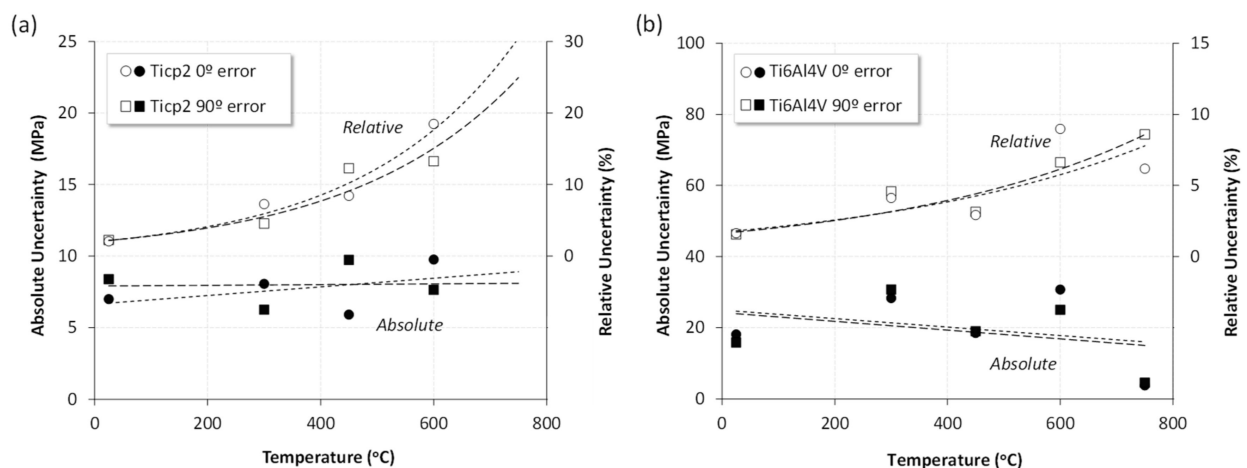


Figure 10. Average relative and absolute typical uncertainty as a function of the temperature. (a) Ticp-2; (b) Ti6Al4V.

The position of the curves establishes whether there is a symmetric or asymmetric response under tensile and compressive stress states. Thus, for the Ticp2 alloy, the asymmetric behavior is mainly observed for the rolling direction at room temperature (Figure 8a). For the transversal direction, the asymmetry remains until 450 °C. The same tendency can be seen for the Ti6Al4V alloy. These results are consistent with the signs detected by Odenberger et al. [36]. In the case of room temperature, the asymmetry detected in the transverse direction is around 10%, which is similar to previous results [37]. From the detailed analysis of the Ticp2 curves, it can be noted that the yield stress is slightly higher in tension than in compression, but immediately afterwards, the strain hardening promotes higher stress for compression in both directions (up to 450 °C). These results are similar to those obtained by Kuwabara et al. [38] for room temperature. For Ti6Al4V, the compression curves are located over the tensile ones when asymmetry appears (Figure 9a,b,d,f). It can be noted that the distance between the tension and compression curves in Figure 9j should be neglected based on the very low absolute values involved. In addition, this last statement is based, as well, on the tendency observed at lower temperatures for 90° and even for the total range of temperatures for 0°. Thus, the difference found in Figure 9j might be the result of an experimental error and not due to an asymmetric behavior of the material. In fact, it was relatively difficult to reach a uniform temperature in the sample during the test at such high temperature.

These results are consistent with those obtained by Battaini et al. [15], which demonstrated the contribution of twinning in the total strain undergone by pure titanium under compression as a function of the temperature. They observed that the contribution of twinning decreased rapidly with the temperature in the rolling direction. However, for the transversal direction of the plate, this contribution continues until higher temperatures (300–400 °C). In view of these results, a direct relationship can be established between T-C asymmetric behavior and the twinning density in the material.

Experimentally, from the friction forces and considering the coefficients of friction involved in the compressive tests, it could be inferred that the lateral pressure applied to the samples was low compared to the principal compressive stress. The biaxial influence was calculated and is shown in Figure 11; the maximum error incurred if biaxial correction is not considered is less than 1%. Accordingly, the equivalent stress can be considered a pure uniaxial compression; that is, no biaxial correction is necessary at any temperature [30,39,40].

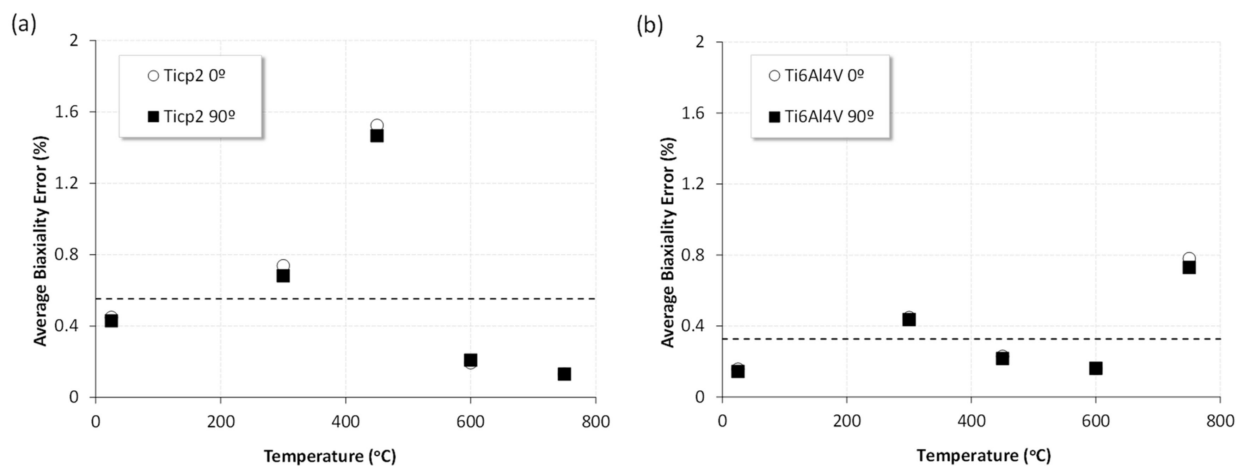


Figure 11. Biaxial influence on the equivalent stress analysis expressed as the value of the average error. (a) Ticp2; (b) Ti6Al4V.

3.2. Asymmetric Tension–Compression Behavior Depending on Temperature and Strain Rates: Preliminary Studies

Figures 12 and 13 depict the influence of the strain rate on the asymmetric compression–tensile behavior at different temperatures. These figures show that the higher the strain rate, the more conservative the asymmetric behavior, i.e., the asymmetry effect is prolonged to higher temperatures. For example, this effect can be clearly observed in Figures 12h and 13h, where the symmetry only exists at the lowest strain rate. For greater clarification, Figure 14 depicts the asymmetry tendency with temperature and strain rate. Specifically, the values for 0.002 s^{-1} , which were previously analyzed in detail (Section 3.1), were extracted from the correlation surfaces. Again, these results might be related to the twin density existing in the material. Nemat-Nasser et al. [13] described the contribution of twinning as a function of the strain rate for different temperatures in compression tests of extruded pure titanium and found a direct correlation with the strain rate, that is, the higher the strain rate, the higher the contribution of twinning.

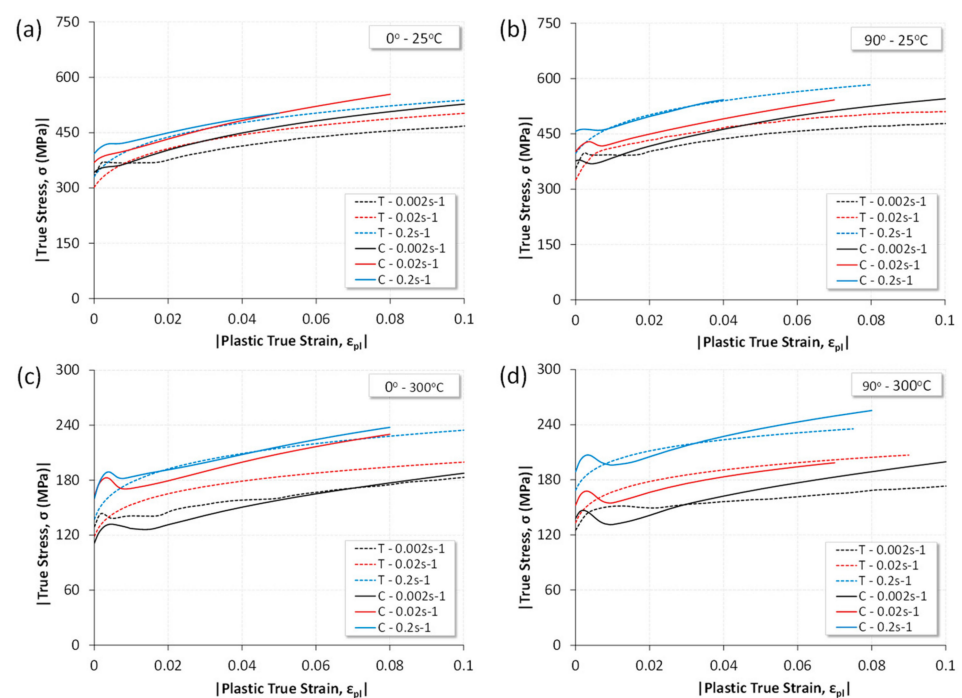


Figure 12. Cont.

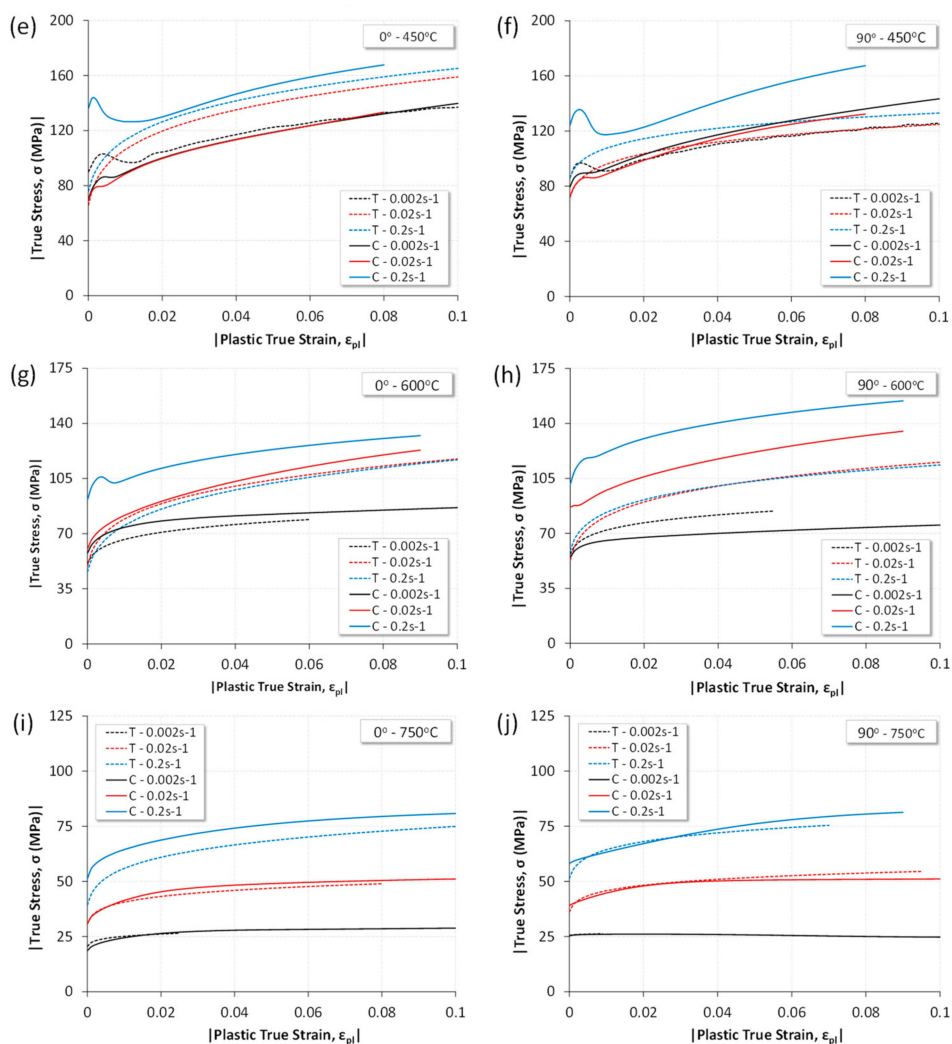


Figure 12. Tension and compression behavior of Ticp2 at temperatures of 25, 300, 450, 600, and 750 °C, and strain rates of 0.002, 0.02, and 0.2 s⁻¹. (a,c,e,g,i) Mechanical behavior in rolling direction (0°); (b,d,f,h,j) Mechanical behavior in transverse direction (90°).

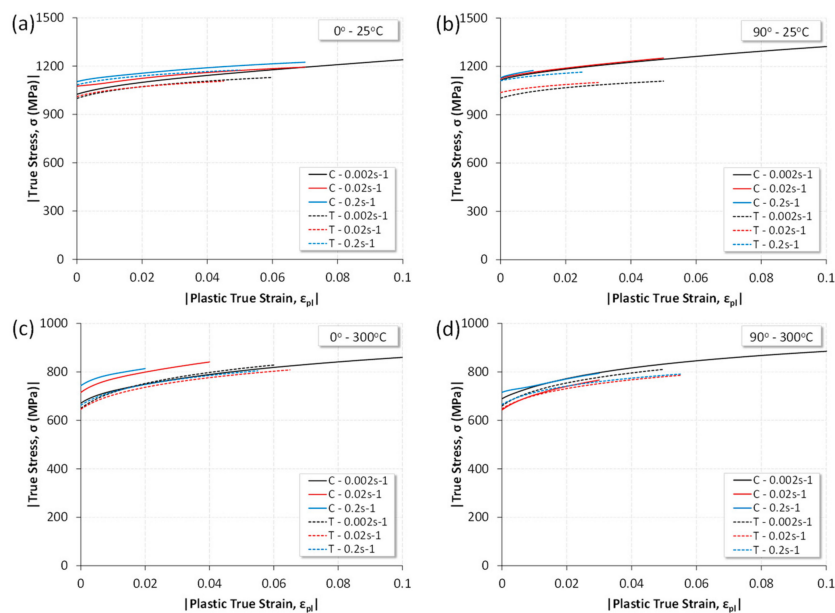


Figure 13. Cont.

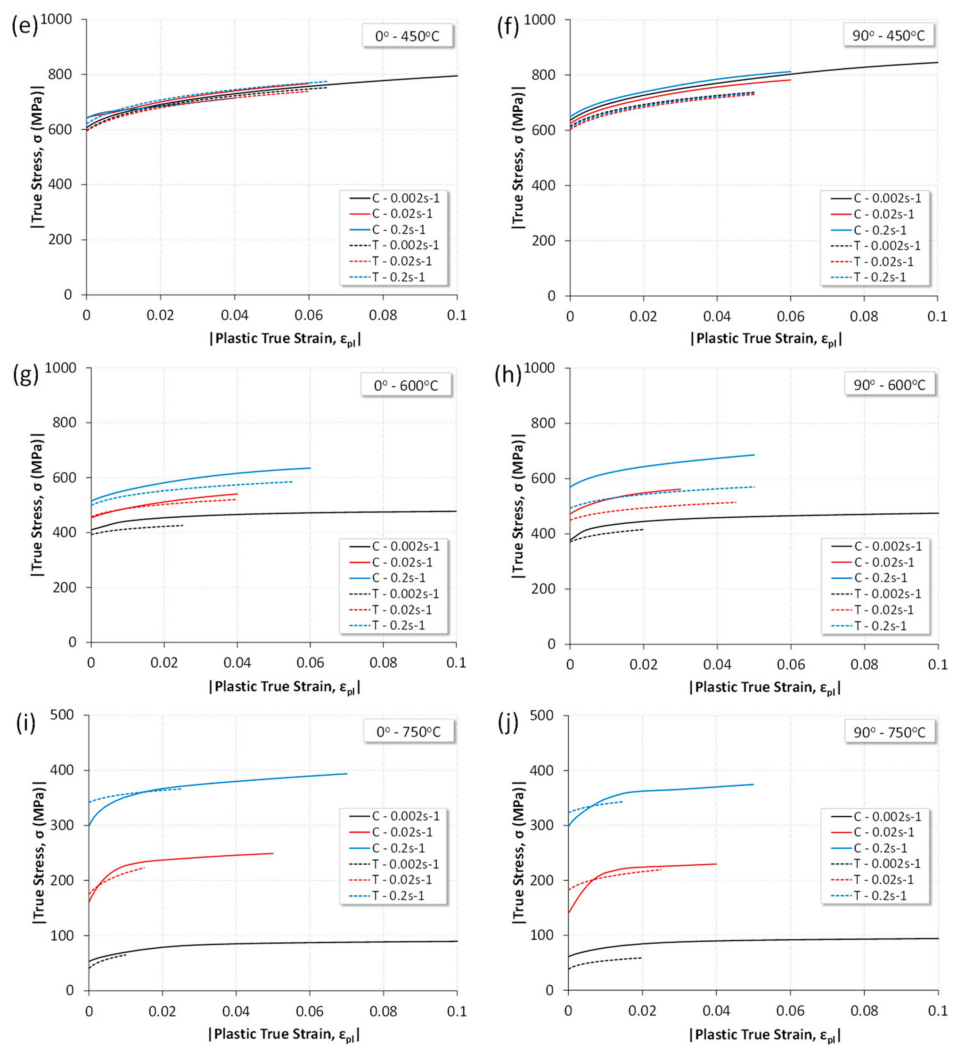


Figure 13. Tension and compression behavior of Ti6Al4V at temperatures of 25, 300, 450, 600, and 750 °C, and strain rates of 0.002, 0.02, and 0.2 s⁻¹. (a,c,e,g,i) Mechanical behavior in rolling direction (0°); (b,d,f,h,j) Mechanical behavior in transverse direction (90°).

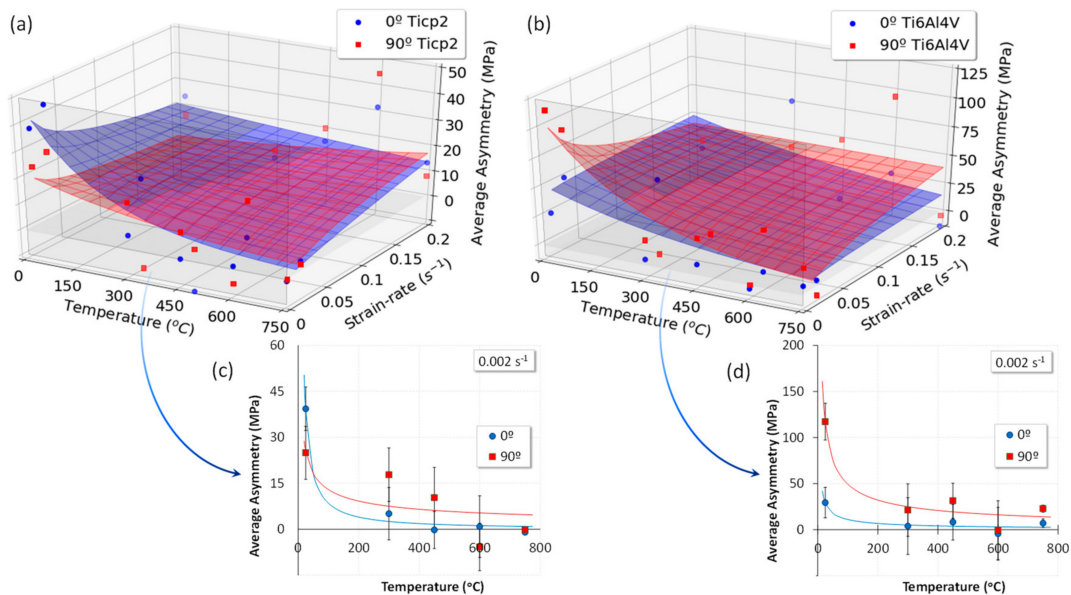


Figure 14. Average asymmetry as a function of the temperature and strain-rate. (a) Ticp2; (b) Ti6Al4V; (c,d) Evolution of the average asymmetry for a strain rate of 0.002 s⁻¹.

3.3. Analysis and Evaluation of the Anisotropy

The values of anisotropy for T1cp2 and Ti6Al4V were experimentally obtained for tensile and compressive stresses at different temperatures (Figure 15).

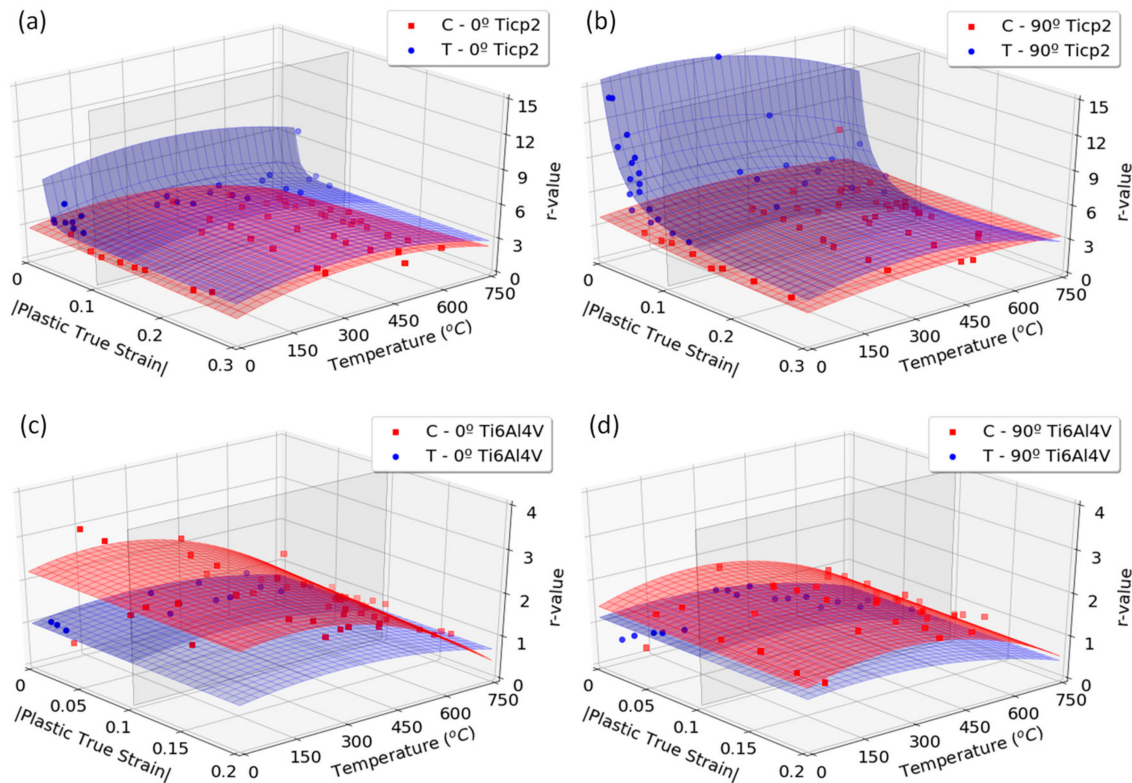


Figure 15. r -values obtained at 0.002 s^{-1} under tension (T) and compression (C) conditions. (a) T1cp2 0° ; (b) T1cp2 90° ; (c) Ti6Al4V 0° ; and (d) Ti6Al4V 90° .

The tensile r -values for T1cp2 depend on the plastic strain at all analyzed temperatures, especially for the transverse direction, as can be observed in Figure 15a,b (blue surfaces). In this direction, the anisotropy is very high at the onset of the plastic period with a decreasing tendency to reach a stable value at high strain values, near the necking point. This transient evolution is less severe in the rolling direction (Figure 15a). Although there are no references in the literature for tensile anisotropy strain evolution at high temperatures, these results are consistent with those found by other authors at room temperature [41]. Moreover, although some dispersion data can be found in the literature [22,42–44], the results for T1cp2 obtained herein were higher than those reported by other authors. This discrepancy of the results might be explained by the use of different criteria for expressing the values, that is, whether the stable anisotropy value or the average value in a range of strains is considered. Nevertheless, other aspects can affect the anisotropy, such as the specific rolling route or rolling program followed by the material sheet. Some authors underline the significant differences this aspect can generate [44,45].

Furthermore, the anisotropy results obtained under the tensile condition for Ti6Al4V are typically similar to those found in the literature, as shown in Figure 16 [46–50]. There are a limited number of previous studies at warm/high temperatures [46,49,50], and the values found present the same tendency as those obtained in the present work (Figure 15c,d). As can be appreciated, no transient anisotropy strain evolution phenomenon appears.

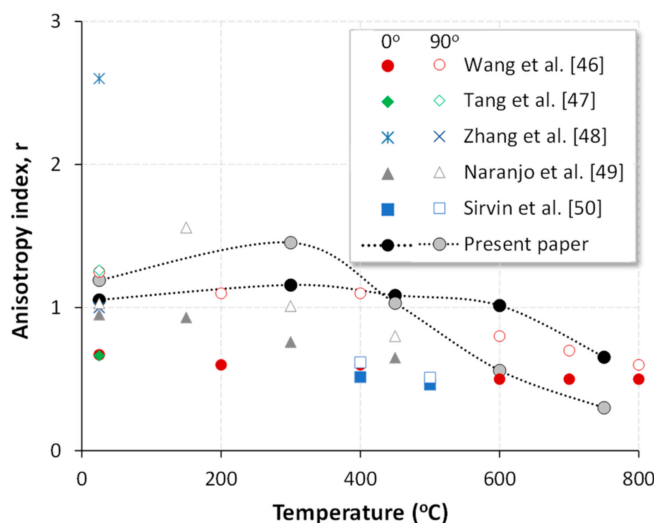


Figure 16. Ti6Al4V r-values obtained in this paper compared to those obtained by previous authors.

Due to the non-existence of the necking phenomenon in compression tests, the anisotropy could be evaluated over a large range of strains, as observed in the red surfaces of Figure 15. The r-values are more homogeneous at each temperature condition for the two materials experimented.

In view of the anisotropy evolution, the r-values were extracted at a strain reference of 0.1. These are shown in Figure 17, where the evolution of stable and representative r-values can be clearly visualized with the temperature and direction under tension and compression states. Drawing on the above discussion, it can be stated that the anisotropy values under tension condition can be extrapolated to the compressive states for temperatures above 450 °C. However, for lower temperatures, the expected behavior of the sheet will be conditioned by the stress state. This difference in behavior must be justified based on the combination of different existing deformation mechanisms as a function of the direction in the sheet and the direction of the applied loads. This causes the material to flow in a preferential way, originating differences in the width strain and in the thickness strain depending on if the stress state is tension or compression. Therefore, the anisotropy index will be different [23]. The highest values of compression anisotropy obtained for Ti6Al4V are consistent with the highest anisotropy detected by Tuninetti et al. [37].

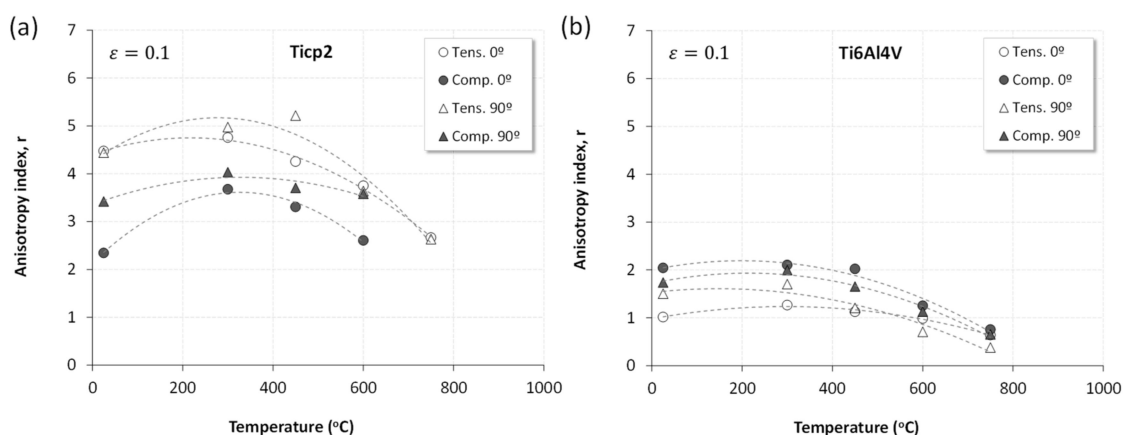


Figure 17. Tensile and compressive anisotropy r-values in the rolling (0°) and transverse (90°) directions as a function of temperature for $\epsilon = 0.1$. (a) Ticp2 0.002 s^{-1} ; (b) Ti6Al4V 0.002 s^{-1} .

4. Modeling the Experimental Results

Traditional mechanical behavior models consider tensile and compression states separately, defining the corresponding equations and applying them by means of the equivalent stress–strain criterion employed. Eventually, it may be useful to have a complete behavior model, especially for the programming of analytical procedures in applications, such as bending, where the stress system is typically a tensile–compression one [51,52]. Moreover, this proposal would simplify the material modeling with complex flow surfaces or loci dependent of the plastic work [21]. Thus, using the experimental data, a mechanical model for the tensile–compression field of the material is proposed. This model is based on a modifier-factor, ζ , which permits the asymmetric behaviour observed for the titanium alloys to be taken into account. The ζ -factor is valid for all typical behavior equations to which it can be applied, such as the Swift or Fields–Backofen functions, for example, and it turns the tensile model into the expected compression one.

For every temperature and strain rate, it was observed that the asymmetry obtained in tension–compression showed a linear increment in stress, σ_a , with the strain in all cases (Figure 18a), which can be established according to Equation (3), where K_a and σ_{a0} are the coefficients of the linear evolution of the asymmetry. To apply the indicated correction Equation (3) only for the compression strains, the parameter f_{c-t} had to be considered, as shown in Equation (4). The non-dimensional exponent Q in Equation (4) adopts a high value to turn f_{ct} into 0 or 1 if the strain is positive or negative, respectively. That is, f_{c-t} behaves, in practice, similarly to the typical Heaviside step function (Figure 18b). In this way, ζ results from the product of f_{c-t} and σ_a .

$$\sigma_a = K_a \varepsilon + \sigma_{a0} \tag{3}$$

$$f_{c-t} = \frac{1}{1 + e^{Q\varepsilon}} \tag{4}$$

Potential functions, which are traditionally considered to define mechanical models, do not allow negative input values to be applied. For this reason, a new function parameter, χ , was defined, Equation (5), which allows us to transform the tensile function into a negative stress–strain curve (Figure 18b), which is typically located in the Cartesian third quadrant.

$$\chi = \frac{2}{\pi} \arctg(Q\varepsilon) \tag{5}$$

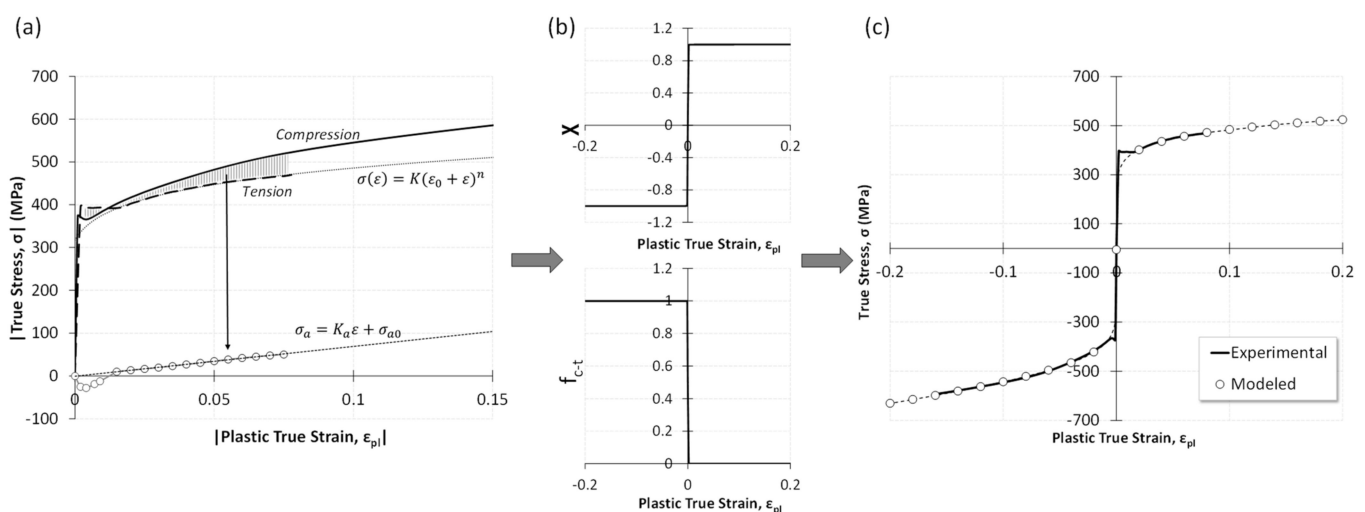


Figure 18. Tension–compression fitting by the modified Swift function, as shown in Equation (8). Case: Tic2 90° 25 °C 0.002 s^{−1}. (a) Tension–Compression difference and fitting according to equation 3; (b) Definition of switching functions (Equations (4) and (5)); (c) Agreement between the proposed model (Equation (7)) and experimental data.

Thus, the T-C model is written in Equation (6) for a general behavior function, $\sigma(\varepsilon)$, or in more detail, in Equation (7), if a Swift type of function is selected. Finally, the proposed model is shown in Figure 18c.

$$\sigma_{t-c}(\varepsilon) = \zeta + \chi \cdot \sigma(\varepsilon) \quad (6)$$

$$\sigma_{t-c} = \frac{1}{1 + e^{Q\varepsilon}} (K_a \varepsilon + \sigma_{a0}) + \frac{2}{\pi} \arctan(Q\varepsilon) K |\varepsilon_0 + \varepsilon|^n \quad (7)$$

The temperature and strain rate should be included in the general function in Equation (6). For this, the ζ -factor must be expressed as a function of those variables. Thus, K_a and σ_{a0} should be correlated with temperature and strain rate (Figure 19). In this way, Equations (8)–(10) depict the functions obtained, where T is the temperature (in K), α_{ij} are functions of the strain rate, and A_{ij} and B_{ij} are constants.

$$\sigma_{a0} = \alpha_{a1} e^{\alpha_{a2}T} \quad (8)$$

$$K_a = \alpha_{k1} e^{\alpha_{k2}T} \quad (9)$$

$$\alpha_{ij} = A_{ij} \ln \dot{\varepsilon} + B_{ij} \quad (10)$$

Finally, the global asymmetry-modifier factor, ζ , is expressed according to Equation (11).

$$\zeta = f_{c-t} \left[\alpha_{a1} e^{\alpha_{a2}T} \varepsilon + \alpha_{k1} e^{\alpha_{k2}T} \right] \quad (11)$$

Nevertheless, to model the material behavior at any temperature and strain rate, it is necessary to use an equivalent tensile stress–strain function including these variables, $\sigma(\varepsilon, T, \dot{\varepsilon})$. For this purpose and taking into account estimations carried out with different constitutive models [53], a modified Fields–Backofen function was finally selected, Equations (12)–(15), where C_i , D_i , and F_i are constants. The parameters of this function were estimated by using a pre-adjustment procedure based on the progressive evaluation of the different variables involved in the law. Once the pre-model was obtained, an accurate fit was carried out by using an iterative process to minimize the global quadratic error implied.

$$\sigma = K \varepsilon^n \dot{\varepsilon}^m \quad (12)$$

$$K = C_1 e^{C_2 T} \quad (13)$$

$$n = D_1 + D_2 \ln(\dot{\varepsilon}) + D_3 e^{D_4 T} \quad (14)$$

$$m = F_1 e^{F_2 T} \quad (15)$$

Finally, the model proposed for the two materials under study is shown in Equation (16), and the values of the coefficients involved are shown in Table 2.

$$\sigma_{t-c}(\varepsilon, T, \dot{\varepsilon}) = f_{c-t} \left[\alpha_{a1} e^{\alpha_{a2}T} \varepsilon + \alpha_{k1} e^{\alpha_{k2}T} \right] + \chi K \varepsilon^n \dot{\varepsilon}^m \quad (16)$$

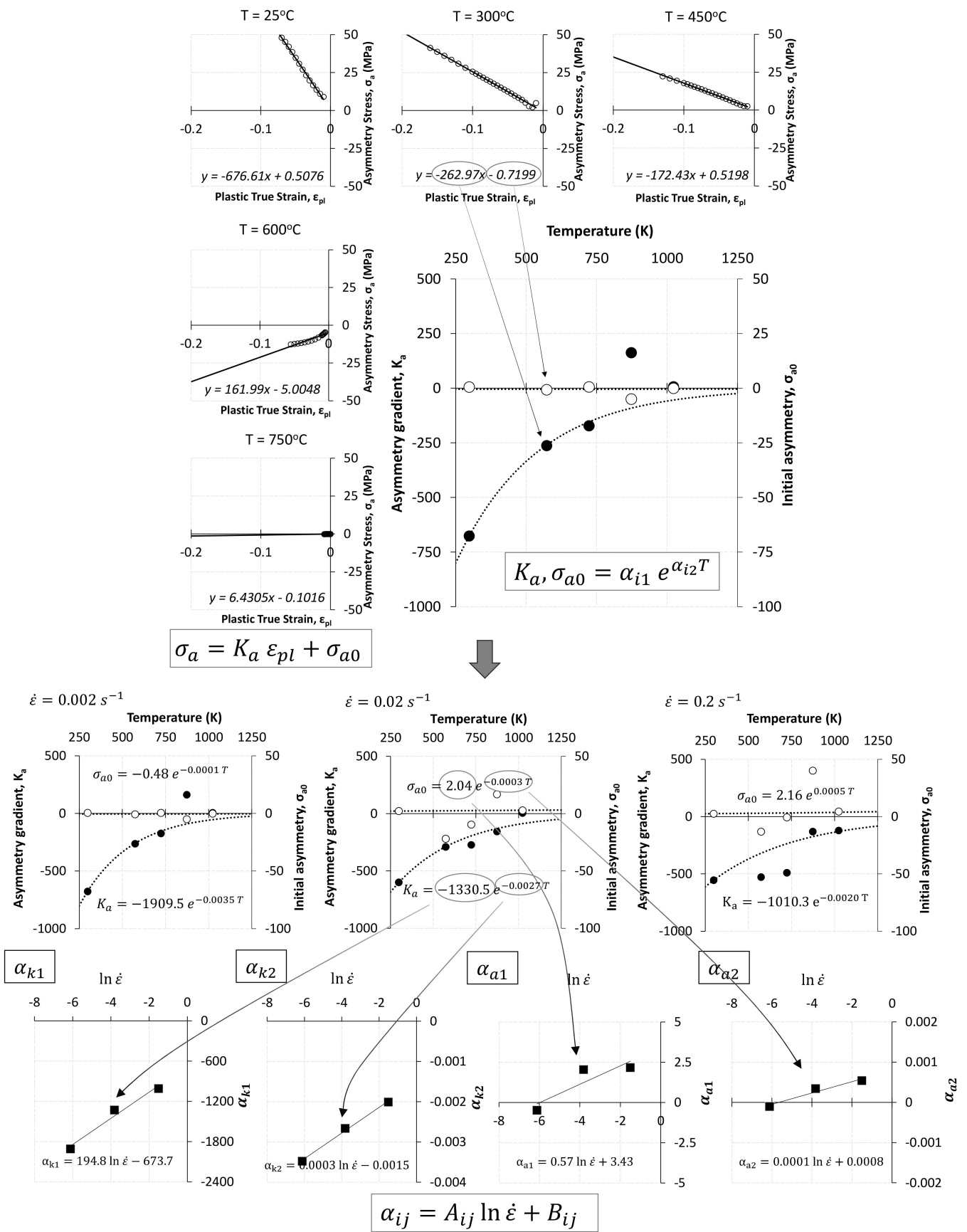


Figure 19. Development of the tension–compression (T-C) asymmetry model as a function of temperature and strain rate. Case: Ticp2 90°.

Table 2. Material parameters of the asymmetric constitutive model for Ticip2 and Ti6Al4V.

| Material | Direction | A_{a1} ($\frac{\text{MPa}}{\text{ins}^{-1}}$) | B_{a1} (MPa) | A_{a2} (K^{-1}) | B_{a2} (K^{-1}) | A_{k1} ($\frac{\text{MPa}}{\text{ins}^{-1}}$) | B_{k1} (MPa) | A_{k2} (K^{-1}) | B_{k2} (K^{-1}) | Q |
|----------|-----------|--|-------------------|---------------------------------|---------------------------------|--|-------------------|---------------------------------|---------------------------------|--------|
| Ticip2 | 0° | 1.428 | 8.786 | 0.050 | -2.13×10^{-6} | 1.553 | 115167.7 | -1.25×10^{-5} | -0.017 | 10,000 |
| | 90° | 1.428 | 8.786 | 0.050 | -2.13×10^{-6} | 1.553 | 114321.7 | -1.25×10^{-5} | -0.018 | 10,000 |
| Ti6Al4V | 0° | 1.428 | 8.786 | 0.050 | -3.84×10^{-6} | 2.389 | 2491.76 | -1.92×10^{-4} | -0.005 | 10,000 |
| | 90° | 49.667 | 45.919 | 8.59×10^{-4} | 1.80×10^{-3} | -255.98 | 7.94 | -0.082 | -0.507 | 10,000 |

| Material | Direction | C_1 (MPa·s) | C_2 (K^{-1}) | D_1 | D_2 ($\frac{1}{\text{ins}^{-1}}$) | D_3 | D_4 (K^{-1}) | F_1 | F_2 (K^{-1}) |
|----------|-----------|------------------|------------------------------|-------|--|------------------------|------------------------------|-----------------------|------------------------------|
| Ticip2 | 0° | 1558.61 | -0.003 | 0.088 | -0.009 | -7.43×10^{-5} | 1.53×10^{-4} | 0.050 | -0.330 |
| | 90° | 1657.95 | -0.003 | 0.051 | -0.011 | -7.44×10^{-5} | 1.53×10^{-4} | 0.050 | -0.330 |
| Ti6Al4V | 0° | 1792.25 | -0.001 | 0.021 | -0.003 | -8.26×10^{-5} | 1.54×10^{-4} | 4.33×10^{-7} | 0.013 |
| | 90° | 1746.26 | -0.001 | 0.005 | -0.004 | -8.72×10^{-5} | 1.55×10^{-4} | 4.33×10^{-7} | 0.013 |

The experimental and modeled data are compared in Figure 20 for Ticip2 and Ti6Al4V and for the transversal direction. A reasonable agreement can be appreciated between them for all the ranges of temperature and strain rates implemented. In fact, the lack of fitting detected in particular cases of the compression functions is directly derived from the deficiency existent in the standard constitutive model selected (first Cartesian quadrant). Moreover, the modified constitutive model, based on the Fields–Backofen model performed, yielded better results than those obtained by traditional proposals. However, the minor deficiencies detected in the tensile adjustments would be corrected by applying specifically developed models that are capable of adopting the marked thermal softening of this kind of material [53]. In sum, the agreement of the proposed model Equation (16) is highly satisfactory, as it allows the asymmetry existent in compression to be reproduced.

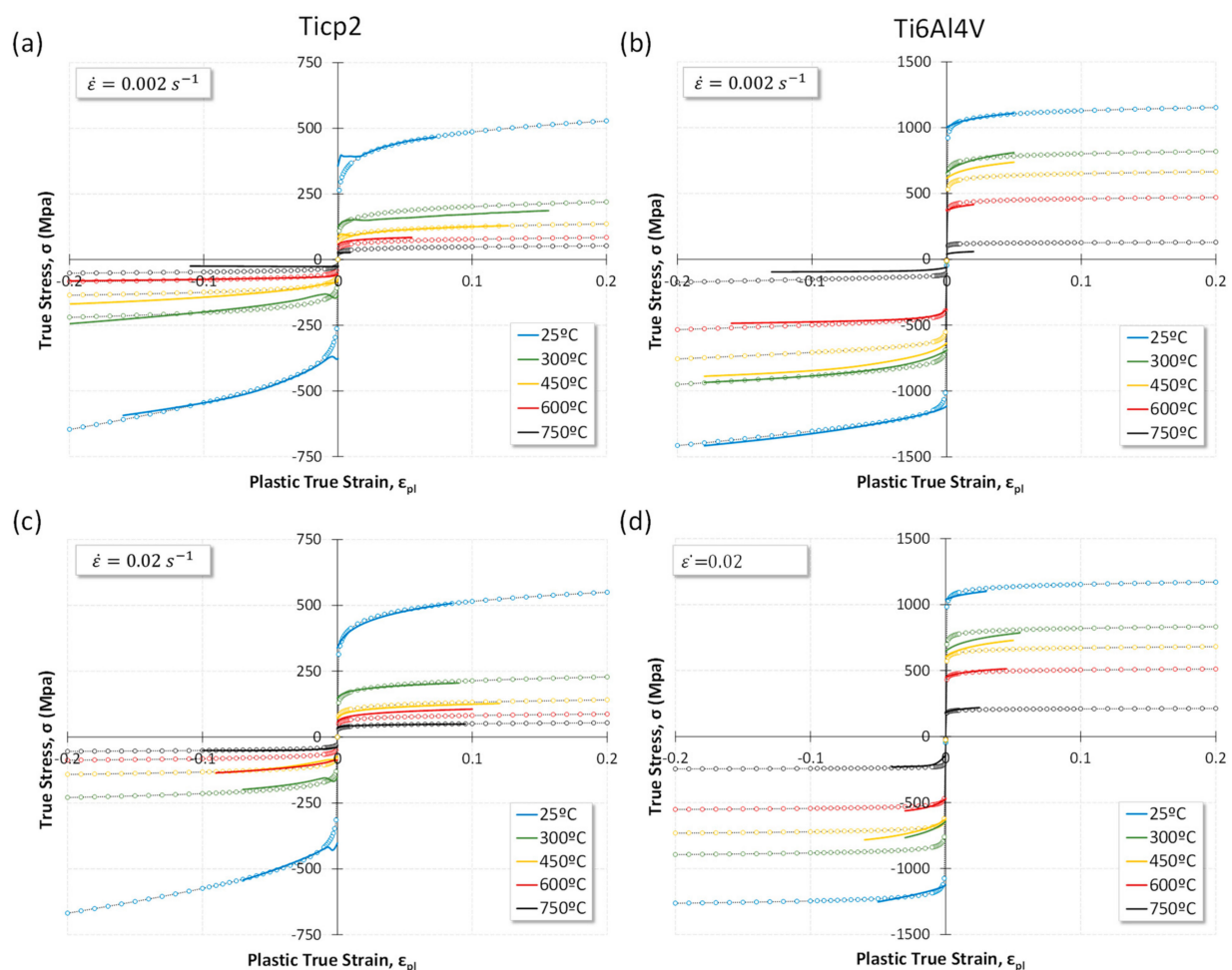


Figure 20. Cont.

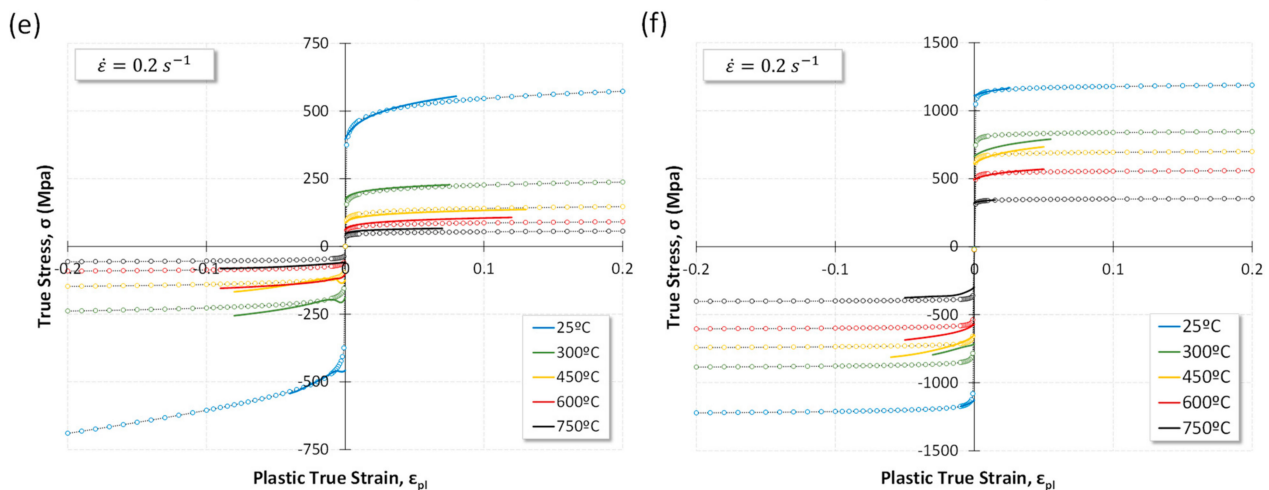


Figure 20. Experimental (continuous trace) and modeling (dotted line) T-C functions for TiCP2 (a,c,e), and Ti6Al4V (b,d,f); the results correspond to TD (90°).

5. Conclusions

The results obtained in this research validate the method previously proposed by the authors, demonstrating the possibility of testing sheet metals under in-plane compressive stress and high temperatures (up to 750 °C). Under these test conditions, T-C asymmetry and compression anisotropy for TiCP2 and Ti6Al4V were determined, being the primary novelty of this work. In more detail, the following aspects can be underlined:

- The T-C asymmetry observed allows us to affirm that this phenomenon decreases with temperature and depends on the rolling direction. In the transverse direction, the asymmetry remains until higher temperatures (450 °C) are reached compared to the rolling direction. The strain rate seems to delay this effect. In addition, the asymmetry value obtained herein and the evolution of twinning density for pure titanium, as detected by other authors, are parallel phenomena that seem to behave in the same way as a function of the temperature and the strain rate. This statement might provide some light about the causes of asymmetry. Nevertheless, this point should be confirmed later on.
- The anisotropy for the mentioned conditions was determined, and it has been proven that under a compression state, the values are clearly different from those obtained by uniaxial tensile tests. In a deeper analysis, no pronounced anisotropy transient behavior with the strain has been found in compression, with the evolution of this parameter being more uniform than those obtained in some cases under tension. Nevertheless, for the highest temperatures, the r-values tend to be similar for both stress states.
- In view of the evolution of the anisotropy and asymmetry phenomena, it can be established that the traditionally assumed symmetrical behavior would not be considered for temperatures lower than 450 °C.
- An asymmetry-modifier parameter was defined to extend the traditional material constitutive models that permit the material behavior to be predicted for the whole field of tension–compression strains. The model was tested with an adapted Fields–Backofen equation, and a good agreement with the experimental results was obtained for all test conditions.

Author Contributions: Conceptualization, J.A., V.M. and A.M.-M.; methodology, J.A., V.M. and A.M.-M.; software, J.A. and F.G.-S.; validation, J.A., V.M. and A.M.-M.; formal analysis, J.A., V.M. and A.M.-M.; investigation, J.A., V.M., A.M.-M., J.C. and J.A.N.; resources, A.M.-M., J.C. and J.A.N.; data curation, J.A. and F.G.-S.; writing—original draft preparation, J.A., V.M., A.M.-M. and J.C.; writing—review and editing, J.A., V.M. and A.M.-M.; visualization, J.A. and F.G.-S.; supervision,

V.M. and A.M.-M.; project administration, V.M.; funding acquisition, V.M. All authors have read and agreed to the published version of the manuscript.

Funding: This research was funded the Regional Research Plan's financial support promoted by the Government of Castilla-La Mancha and FEDER funds: project PREJCCM2016/13.

Institutional Review Board Statement: Not applicable

Informed Consent Statement: Not applicable.

Data Availability Statement: The data presented in this study are available on request from the corresponding author. The data are not publicly available because they are part of an active research.

Conflicts of Interest: The authors declare no conflict of interest. The funders had no role in the design of the study; in the collection, analyses, or interpretation of data; in the writing of the manuscript, or in the decision to publish the results.

References

- Odenberger, E.L.; Oldenburg, M.; Thilderkvist, P.; Stoehr, T.; Lechler, J.; Merklein, M. Tool development based on modelling and simulation of hot sheet metal forming of Ti-6Al-4V titanium alloy. *J. Mater. Process. Technol.* **2011**, *211*, 1324–1335. [\[CrossRef\]](#)
- Mosecker, L.; Göttmann, A.; Saeed-Akbari, A.; Bleck, W.; Bambach, M.; Hirt, G. Deformation mechanisms of Ti6Al4V sheet material during the incremental sheet forming with laser heating. *Key Eng. Mater.* **2013**, *549*, 372–380. [\[CrossRef\]](#)
- Rack, H.J.; Qazi, J.I. Titanium alloys for biomedical applications. *Mater. Sci. Eng. C* **2006**, *26*, 1269–1277. [\[CrossRef\]](#)
- Odenberger, E.L.; Pederson, R.; Oldenburg, M. Finite element modeling and validation of springback and stress relaxation in the thermo-mechanical forming of thin Ti-6Al-4V sheets. *Int. J. Adv. Manuf. Technol.* **2019**, *104*, 3439–3455. [\[CrossRef\]](#)
- Hama, T.; Nagao, H.; Kobuki, A.; Fujimoto, H.; Takuda, H. Work-hardening and twinning behaviors in a commercially pure titanium sheet under various loading paths. *Mater. Sci. Eng. A* **2015**, *620*, 390–398. [\[CrossRef\]](#)
- Tirry, W.; Nixon, M.; Cazacu, O.; Coghe, F.; Rabet, L. The importance of secondary and ternary twinning in compressed Ti. *Scr. Mater.* **2011**, *64*, 840–843. [\[CrossRef\]](#)
- Salem, A.A.; Kalidindi, S.R.; Doherty, R.D.; Semiatin, S.L. Strain hardening due to deformation twinning in α -titanium: Mechanisms. *Metall. Mater. Trans. A* **2006**, *37*, 259–268. [\[CrossRef\]](#)
- Lin, R.; Hao, Y.; Zhang, B.; Zhang, S.; Chi, C.; Shen, J. Tension-compression asymmetry in yielding and strain hardening behavior of CP-Ti at room temperature. *Mater. Sci. Eng. A* **2017**, *707*, 172–180. [\[CrossRef\]](#)
- Roth, A.; Lebyodkin, M.A.; Ledebkina, T.A.; Lecomte, J.-S.; Richeton, T.; Amouzou, K.E.K. Mechanisms of anisotropy of mechanical properties of α -titanium in tension conditions. *Mater. Sci. Eng. A* **2014**, *596*, 236–243. [\[CrossRef\]](#)
- Tirry, W.; Coghe, F.; Bouvier, S.; Gasperini, M.; Rabet, L.; Schryvers, D. A multi-scale characterization of deformation twins in Ti6Al4V sheet material deformed by simple shear. *Mater. Sci. Eng. A* **2010**, *527*, 4136–4145. [\[CrossRef\]](#)
- Yoo, M.H.; Morris, J.R.; Ho, K.M.; Agnew, S.R. Nonbasal deformation modes of HCP metals and alloys: Role of dislocation source and mobility. *Metall. Mater. Trans. A* **2002**, *33*, 813–822. [\[CrossRef\]](#)
- Gilles, G.; Hammami, H.; Libertiaux, V.; Cazacu, O.; Yoon, J.H.; Kuwabara, T.; Habraken, A.M.; Duchene, L. Experimental characterization and elasto-plastic modeling of the quasi-static mechanical response of TA-6V at room temperature. *Int. J. Solids Struct.* **2011**, *48*, 1277–1289. [\[CrossRef\]](#)
- Nemat-Nasser, S.; Guo, W.G.; Cheng, J.Y. Mechanical properties and deformation mechanisms of a commercially pure titanium. *Acta Mater.* **1999**, *47*, 3705–3720. [\[CrossRef\]](#)
- Becker, H.; Pantleon, W. Work-hardening and deformation mechanism maps during tensile deformation of commercially pure titanium. *Comput. Mater. Sci.* **2013**, *76*, 52–59. [\[CrossRef\]](#)
- Battaini, M.; Pereloma, E.V.; Davies, C.H.J. Effect of orientation and temperature on the mechanical properties of commercially pure titanium. *Adv. Mater. Res.* **2007**, *15–17*, 941–946. [\[CrossRef\]](#)
- Paton, N.E.; Backofen, W.A. Plastic deformation of titanium at elevated temperatures. *Metall. Trans.* **1970**, *1*, 2839–2847.
- Zeng, Z.; Zhang, Y.; Jonsson, S. Deformation behaviour of commercially pure titanium during simple hot compression. *Mater. Des.* **2009**, *30*, 3105–3111. [\[CrossRef\]](#)
- Nixon, M.E.; Cazacu, O.; Lebensohn, R.A. Anisotropic response of high-purity α -titanium: Experimental characterization and constitutive modeling. *Int. J. Plast.* **2010**, *26*, 516–532. [\[CrossRef\]](#)
- Battaini, M.; Pereloma, E.V.; Davies, C.H.J. Orientation effect on mechanical properties of commercially pure titanium at room temperature. *Metall. Mater. Trans. A* **2007**, *38*, 276–285. [\[CrossRef\]](#)
- Liu, K.; Dong, X.; Xie, H.; Wu, Y.; Peng, F.; Chen, F. Asymmetry in the hot deformation behavior of AZ31B magnesium sheets. *Mater. Sci. Eng. A* **2016**, *659*, 198–206. [\[CrossRef\]](#)
- Raemy, C.; Manopulo, N.; Hora, P. On the modelling of plastic anisotropy, asymmetry and directional hardening of commercially pure titanium: A planar Fourier series based approach. *Int. J. Plast.* **2017**, *91*, 182–204. [\[CrossRef\]](#)
- Manopulo, N.; Raemy, C.; Hora, P. A flexible modelling approach for capturing plastic anisotropy and strength differential effects exhibited by commercially pure titanium. *Int. J. Solids Struct.* **2018**, *151*, 91–98. [\[CrossRef\]](#)

23. Zhou, P.; Beeh, E.; Friedrich, H.E. Influence of tension-compression asymmetry on the mechanical behavior of AZ31B magnesium alloy sheets in bending. *J. Mater. Eng. Perform.* **2016**, *25*, 853–865. [[CrossRef](#)]
24. Nixon, M.E.; Lebenshon, R.A.; Cazacu, O.; Liu, C. Experimental and finite-element analysis of the anisotropic response of high-purity x-titanium in bending. *Acta Mater.* **2010**, *58*, 5759–5767. [[CrossRef](#)]
25. Barros, P.D.; Alves, J.L.; Oliveira, M.C.; Menezes, L.F. Modeling of tension-compression asymmetry and orthotropy on metallic materials: Numerical implementation and validation. *Int. J. Mech. Sci.* **2016**, *114*, 217–232. [[CrossRef](#)]
26. Boger, R.K.; Wagoner, R.H.; Barlat, F.; Lee, M.G.; Chung, K. Continuous, large strain, tension/compression testing of sheet material. *Int. J. Plast.* **2005**, *21*, 2319–2343. [[CrossRef](#)]
27. Kuwabara, T.; Kumano, Y.; Ziegelheim, J.; Kurosaki, I. Tension-compression asymmetry of phosphor bronze for electronic parts and its effect on bending behavior. *Int. J. Plast.* **2009**, *25*, 1759–1776. [[CrossRef](#)]
28. Piao, K.; Lee, J.K.; Kim, J.H.; Kim, H.Y.; Chung, K.; Barlat, F.; Wagoner, R.H. A sheet tension/compression test for elevated temperature. *Int. J. Plast.* **2012**, *38*, 27–46. [[CrossRef](#)]
29. Lee, M.G.; Kim, J.H.; Kim, D.; Seo, O.S.; Nguyen, N.T.; Kim, H.Y. Anisotropic hardening of sheet metal at elevated temperature: Tension-compressions test development and validation. *Exp. Mech.* **2013**, *53*, 1039–1055. [[CrossRef](#)]
30. Ayllón, J.; Miguel, V.; Martínez-Martínez, A.; Coello, J.; Naranjo, J.A. A new approach for obtaining the compression behavior of anisotropic sheet metals applicable to a wide range of test conditions. *Metals* **2020**, *10*, 1374. [[CrossRef](#)]
31. ISO 6892-2: 2018 *Metallic Materials—Tensile Testing—Part 2: Method of Test at Elevated Temperature*; ISO: Geneva, Switzerland, 2018.
32. ISO 10113: 2016 *Metallic Materials—Sheet and Strip—Determination of Plastic Strain Ratio*; ISO: Geneva, Switzerland, 2016.
33. Podgornik, B.; Kafexhiu, F.; Kosec, T.; Jerina, J.; Kalin, M. Friction and anti-galling properties of hexagonal boron nitride (h-BN) in aluminium forming. *Wear* **2017**, *388–389*, 2–8. [[CrossRef](#)]
34. Guo, J.; Zhan, M.; Fu, M.W.; Gao, P.F.; Ma, F. Extrapolation based constitutive modeling of flow stress of titanium alloy sheet under hot-working condition. *Mater. Des.* **2018**, *154*, 96–107. [[CrossRef](#)]
35. Lin, P.; He, Z.; Yuan, S.; Shen, J. Tensile deformation behavior of Ti-22Al-25Nb alloy at elevated temperatures. *Mater. Sci. Eng. A* **2012**, *556*, 617–624. [[CrossRef](#)]
36. Odenberger, E.L.; Hertzman, J.; Thilderkvist, P.; Merklein, M.; Kuppert, A.; Stöhr, T.; Lechler, J.; Oldenburg, M. Thermo-mechanical sheet metal forming of aero engine components in Ti-6Al-4V-PART 1: Material characterisation. *Int. J. Mater. Form.* **2013**, *6*, 391–402. [[CrossRef](#)]
37. Tuninetti, V.; Gilles, G.; Milis, O.; Pardoën, T.; Habraken, A.M. Anisotropy and tension-compression asymmetry modeling of the room temperature plastic response of Ti-6Al-4V. *Int. J. Plast.* **2015**, *67*, 53–68. [[CrossRef](#)]
38. Kuwabara, T.; Katami, C.; Kikuchi, M.; Shindo, T.; Ohwue, T. Cup drawing of pure titanium sheet finite element analysis and experimental validation. In *Proceedings of the 7th International Conference Numerical Methods in Industrial Forming Processes*; Mori, K., Ed.; Balkema: Lisse, The Netherlands, 2001; p. 781.
39. Cao, J.; Lee, W.; Cheng, H.S.; Seniw, M.; Wang, H.-P.; Chung, K. Experimental and numerical investigation of combined isotropic-kinematic hardening behavior of sheet metals. *Int. J. Plast.* **2009**, *25*, 942–972. [[CrossRef](#)]
40. Lee, M.G.; Kim, D.; Kim, C.; Wenner, M.L.; Wagoner, R.H.; Chung, K. Spring-back evaluation of automotive sheets based on isotropic-kinematic hardening laws and non-quadratic anisotropic yield functions. Part II: Characterization of material properties. *Int. J. Plast.* **2005**, *21*, 883–914.
41. Baral, M.; Hama, T.; Knudsen, E.; Korkolis, Y. Plastic deformation of commercially-pure titanium: Experiments and modeling. *Int. J. Plast.* **2018**, *105*, 164–194. [[CrossRef](#)]
42. Pham, Q.T.; Lee, M.G.; Kim, Y.S. Characterization of the isotropic-distortional hardening model and its application to commercially pure titanium sheets. *Int. J. Mech. Sci.* **2019**, *160*, 90–102. [[CrossRef](#)]
43. Singh, A.; Basak, S.; Prakash, L.; Roy, G.G.; Jha, M.N.; Mascarenhas, M.; Panda, S.K. Prediction of earing defect and deep drawing behavior of commercially pure titanium sheets using CPB06 anisotropy yield theory. *J. Manuf. Process.* **2018**, *33*, 256–267. [[CrossRef](#)]
44. Jianjun, W.; Bao, W.; Weiping, L. Mechanical properties and planar anisotropy of TC1 titanium alloy sheet. *Rare Met. Mater. Eng.* **2017**, *46*, 363–369. [[CrossRef](#)]
45. Liu, D.K.; Huang, G.S.; Gong, G.L.; Wang, G.G.; Pan, F.S. Influence of different rolling routes on mechanical anisotropy and formability of commercially pure titanium sheet. *Trans. Nonferrous Met. Soc. China* **2017**, *27*, 1306–1312. [[CrossRef](#)]
46. Wang, Q.L.; Novella, M.F.; Guiotti, A.; Bruschi, S. Anisotropy influence on flow behaviour and plastic instability of Ti6Al4V sheets deformed in a wide range of temperatures and strain rates. *Proc. Eng.* **2017**, *207*, 2161–2166. [[CrossRef](#)]
47. Tang, B.; Wang, Q.; Guo, N.; Li, X.; Wang, Q.; Ghiotti, A.; Bruschi, S.; Luo, Z. Modeling anisotropic ductile fracture behavior of Ti-6Al-4V titanium alloy for sheet forming applications at room temperature. *Int. J. Solids Struct.* **2020**, *207*, 178–195. [[CrossRef](#)]
48. Zhang, K.; Badreddine, H.; Saanouni, K. Ductile fracture prediction using enhanced CDM model with Lode angle-dependency for titanium alloy Ti-6Al-4V at room temperature. *J. Mater. Process. Technol.* **2020**, *277*, 116462. [[CrossRef](#)]
49. Naranjo, J.A.; Miguel, V.; Martínez, A.; Coello, J.; Manjabacas, M.C. Evaluation of the formability and dimensional accuracy improvement of Ti6Al4V in warm SPIF processes. *Metals* **2019**, *9*, 272. [[CrossRef](#)]
50. Sirvin, Q.; Velay, V.; Bonnaire, R.; Penazzi, L. Mechanical behaviour modelling and finite element simulation of simple part of Ti-6Al-4V sheet under hot/warm stamping conditions. *J. Manuf. Process.* **2019**, *38*, 472–482. [[CrossRef](#)]

-
51. Martinez, A.; Miguel, V.; Coello, J. A new approach to evaluate bending forces for deep-drawing operations of a TRIP700+EBT steel sheet. *Int. J. Mater. Form.* **2018**, *11*, 619–641. [[CrossRef](#)]
 52. Ahn, K. Plastic bending of sheet metal with tension/compression asymmetry. *Int. J. Solids Struct.* **2020**, *204–205*, 65–80. [[CrossRef](#)]
 53. Ayllon, J.; Miguel, V.; Coello, J.; Martinez-Martinez, A. Experimental results and constitutive model of the mechanical behavior of Ti6Al4V alloy at high temperature. *Proc. Manuf.* **2019**, *41*, 723–730.